Water Vapor Transportation into the Tibetan Plateau and Formation Processes of Mesoscale Convective Systems during Monsoon Season

January 2010

Shiori SUGIMOTO

Water Vapor Transportation into the Tibetan Plateau and Formation Processes of Mesoscale Convective Systems during Monsoon Season

A Dissertation Submitted to
the Graduate School of Life and Environmental Sciences,
the University of Tsukuba
in Partial Fulfillment of the Requirements
for the Degree of Doctor of Philosophy in Science

Shiori SUGIMOTO

Abstract

Cloud convections over the Tibetan Plateau (TP) have been attracted attention of many researchers, because latent heat release from them contributes to formation and maintenance of the summer monsoon circulation. The TP is semi-arid region due to inland and high elevation, and water vapor (WV) transport from outside the TP is essential for the active cloud convection. However, it is unclear when and how WV is supplied over the TP. Then, WV transport process was analyzed in 1998 summer using the GAME reanalysis data together with a numerical model, focusing on the large-scale circulation pattern in the Indian monsoon region and the diurnal variation of WV intrusion from south of the Himalayas to the TP. WV advection into the TP was significant in the case of a passing synoptic trough over the plateau, comparing with the case of extension of upper tropospheric anticyclone. Sub-continental scale circulation for those synoptic cases corresponded to the break/active phase of the Indian monsoon. When the upper tropospheric anticyclone was dominant, a cyclonic circulation with a low-pressure area over India prevented the WV intrusion into the TP in the middle troposphere. In the case of trough passage that corresponded with the break phase of Indian monsoon, WV was transported directly from the Arabian Sea to the southern foot of the Himalayas with a northward shift of the low-level monsoon westerly, and it intruded into the southeastern TP. Numerical experiments showed that WV transport process was composed of multiple steps in the case of the passing trough. Moist air mass was supplied by the monsoon westerly flow to the southern foot of the Himalayas at 1500 m above sea level (a.s.l.). The moisture was brought up to south of the TP at about 5500 m a.s.l. during noon to evening due to development of a mixing layer and the enhancement of upslope winds in the southern slope of the Himalayas. In the southeastern TP, moist southwesterlies converged longitudinally with the dry northwesterlies prevailing in the rear of the passing synoptic trough. This convergence area expanded northward from mid-afternoon into the night and disappeared early in the next morning. Formation of the convergence limited the moistening area in the southeastern TP.

Recently, satellite images confirm organization of cloud convections, that is mesoscale convective system (MCS), not only the individual convective clouds. The MCS formed over the eastern TP sometimes becomes trigger of flood the middle and lower reaches of the Yangtze River. In second part of this study, formation mechanism of MCS over the eastern plateau was revealed, focusing on the establishment of sub-plateau-scale convergences affected by the longitudinal surface wetness gradient. Composites of re-analysis data and satellite infrared images showed that large-scale MCSs occurred in the afternoon under the

condition of the eastward expansion of upper tropospheric anticyclone with enhancement of near-surface low pressure in the western plateau. The low-level convergence was systematically formed through the eastward propagation of a thermally induced cyclonic circulation formed in the north-central plateau before the day of the MCS genesis. A numerical model successively simulated the MCS occurrence processes in the eastern plateau with the diurnal evolution of convergences, namely, 1) the formation of wind shear between southwesterlies and northeasterlies over the strong heated land-surface causing a thermal-low in the northwest, 2) the eastward propagation of the vorticity due to steering by upper westerlies in the night, and 3) the MCS genesis by low-level convergence behind the migrated vortex with a convective instability condition over the eastern wet land surface. Numerical sensitivity experiments confirmed that eliminating either the western surface sensible heat flux or the eastern surface latent heat flux prevented the simulation of the MCS genesis. In particular, the enhanced southeast-northwest gradation of the plateau-scale soil moisture distribution could effectively form the MCSs in the eastern plateau during the monsoon season.

Key words: Tibetan Plateau, water vapor transportation, Indian monsoon activity, mesoscale convective systems, land-atmosphere interaction, low vortex, soil moisture gradation

Contents

List of Figures

List of Tables

Chapter 1 Introduction

1.1 Function of the Tibetan Plateau to the monsoon circulation

Tibetan Plateau (TP) with average elevation of 4000 m above sea level (a.s.l) has dynamically and thermodynamically impacts on summer Asian monsoon climate. For the mechanical effect, westerly jet is split into two major streams at lower and middle troposphere until early May, and they are located in north and south of the TP. The southern jet stream prevents ascending motion and precipitation over the northern India (Sato and Kimura, 2007). Besides, orographic stationary wave is formed dynamically in not only winter but also summer. According to the sensitivity experiment removing mountains topography using numerical model, east-west variability of precipitation in the mid-latitude is weakened by small amplitudes of the orographic stationary wave due to changing of storm track (Manabe and Broccoli, 1990).

The thermodynamical effect is primarily responsible for the establishment of the summer monsoon over Asia (Murakami, 1987). The TP heating contributes to reverse of meridional temperature contrast between Eurasian continent and Indian Ocean (Murakami and Ding, 1982; Li and Yanai, 1996) and to form variations of the monsoon circulation. Numerical experiment without TP topography by Hahn and Manabe (1975) could not simulated large-scale monsoon circulation in the lower troposphere, abruptly northward jump of subtropical jet in the upper troposphere, and northward migration of rainfall area in the Asian monsoon region. Ueda and Yasunari (1998) indicated that the timing of Southeast Asian monsoon onset corresponds well with the strong heating phase over the TP and Himalaya, which enhances moist monsoon

westerly in the lower troposphere. According to the recent numerical study by Sato and Kimura (2007), subsidence around the plateau associated with the TP heating suppresses cloud convection over the northern India and retards northward transition of Indian monsoon rainfall.

There are two heat sources over the TP; one is the sensible heat from plateau surface in the middle troposphere, and other is latent heat released from cloud convection. Heat sources and moisture sinks analysis suggested that sensible heat is dominant over the western TP during spring through summer, and contribution of the latent heat from cloud to middle and upper tropospheric heating is same as sensible heat over the eastern TP after monsoon onset (Nitta, 1983; Luo and Yanai, 1984; Yanai et al., 1992; Yanai and Li; 1994, Figure 1.1). Ueda et al. (2003) pointed out that condensation heating generated by convective rainfall near ground surface over the western plateau slope and sensible heating are nearly equal during pre-monsoon season. Therefore, formation mechanism of cloud convection over the TP during summer season has been one of important study object for many researchers.

1.2 Convective activity over the TP

The convective activity over the TP has been revealed mainly using satellite images due to lack of in-situ observation site. Murakami (1983) analyzed deep convective activity in the Western Pacific and southeast Asia, and he identified that significant active cloud convection over the southern TP was intensified (weakened) in the evening (morning), comparing with other regions. Local circulation caused by large scale mountain ranges has been considered to play a fundamental role in thermally induced diurnal convective activities, which dominate in the

southern and southeastern TP (Ueno, 1998; Kurosaki and Kimura, 2002; Fujinami et al., 2005, Figure 1.2). In 1998, Doppler-radar observation which was carried out at Naqu basin during summer monsoon season as a part of Global Energy and Water Cycle Experiment (GEWEX) Asian Monsoon Experiment (GAME/Tibet) project. According this observation, echo tops reached to about 17 km above sea level (a.s.l) with small echo area about 4000 m^2 (Uyeda et al., 2001, Figure 1.3). Their result indicated that latent heat release from cloud convection reached to upper troposphere. Recently, satellite images also confirmed organization of cloud convections, not only the individual convective clouds. Many of the cloud convective clusters were observed extensively over the southern TP in the afternoon and evening (Barros et al., 2004). Precipitation radar (PR) images of Tropical Rainfall Measuring Mission (TRMM) also indicated that precipitation systems with more than 10^4 km^2 occurred over the eastern TP in the afternoon and through the night (Hirose and Nakamura, 2005). According to the statistical analysis of multiple satellite infrared (IR) images by Li et al. (2008), precipitation with convective systems (CSs), which was defined as lower than 245 K of cloud top temperature and larger than 90 km of minimum radius, accounted for more than 60 % of the total precipitation over the eastern TP, and the CSs sometimes migrated to eastern China, South Asia, and the Bay of Bengal (Figure 1.4). Yasunari and Miwa (2006) showed some cases of the eastward movement of the vortexes with cloud convective systems, which were formed by large-scale convergence over the TP, triggered flooding in the middle and lower reaches of the Yangtze River. Systemized cloud convection in the eastern TP provides precipitation over the semi-arid plateau region, changes the surface heat balance, and modifies the weather in the leeside of the plateau.

On the other hand, synoptic disturbance is pointed out for another important precipitation system over the plateau. Ueno et al. (2001) indicated that weak and frequent precipitation occurred over the relatively flat areas such as Naqu basin, and that passage of the synoptic disturbance has possibility to be primary trigger causing major precipitation events. Large-scale low-level convergence induced by passing a synoptic front was suggested for one of the factor of stratiform precipitation formation during evening through night (Shimizu et al., 2001). Occurrence of nighttime precipitation over the central TP was explained by formation of low-level convergence of southwesterlies with easteries, which was caused due to stagnation of the northwesterly winds flowing in the west of the trough at northern and northwestern edge slopes of the plateau (Ueno et al. 2009). Function of synoptic trough to the diurnally induced cloud convection over the plateau should be investigated more.

1.3 Water vapor supply into the TP

The absolute amount of atmospheric moisture over the TP is small compared to that at lower elevations because of low-pressure and low-temperature conditions, although the active cloud convection occurs as described above. Water vapor (WV) supply into the column of the atmosphere is essential for the formation of active cloud convection under the condition with the dry atmospheric environment. However, there is no study described transport process of WV into the TP, explicitly. Two major sources are categorized for the WV supply over the TP; evaporation from land-surface and advection from outside the TP. Using numerical simulations, Numaguti (1999) estimated that the contribution of WV evaporating from the

northern Indian Ocean to the precipitating water over the TP was more than 50 % of all oceanic origins. He also indicated that the recycling rate of precipitation between the atmosphere and the land surface was about 35% over the TP. Based on stable isotope observations, Tian et al. (2001) indicated that oceanic-originated moisture, evaporated from the Bay of Bengal (BoB), was the main source of WV in the southern TP. These results indicate that the WV advection from outside the TP strongly contribute to the water cycle activity over the plateau.

WV transportation from outside the plateau has possibility to be affected by Indian monsoon activity and variability of mid-latitude westerly changing the synoptic condition around the TP. It is well known that the Indian monsoon has an active/break phase with a timescale of about 15 days or 30-50 days and that the precipitation amount increases or decreases over central India in the active or break phase, respectively, of the Indian Monsoon (e.g., Murakami, 1976; Kurishunamurti and Bhalme, 1976; Yasunari, 1979; Yasunari, 1980; Yasunari, 1981; Pant, 1983). The timescale of about 15 days is explained by north-south oscillation of monsoon westerlies (Murakami, 1976; Murakami, 1977). The 40-day timescale is caused by the northward movement of cloud disturbance over the Asian monsoon region (60°-120°E), which is initiated by eastward propagating of clouds corresponded with the Madden-Julian Oscillation (e.g., Yasunari, 1979; Yasunari, 1981; Lau and Chan, 1986). Chang (1981) indicated an inverse correlation between the precipitation amount in central India and that in the central TP with the timescale of about 15 and 40 day. This means that active WV supply into the TP could occur during the break phase of the Indian monsoon. On the other sides, Fujinami and Yasunari (2001, 2004) stated that convective activity over the TP was controlled by intraseasonal variability with

7-20 days timescale which composed by an east-west oscillation of the Tibetan High in the upper troposphere and the southward extension of the mid-troposphere trough. Yamada and Uyeda (2006) focused on the differences in synoptic conditions, such as the prevailing cumulus convection with a dominant Tibetan High (Upper High; UH type) and the passage of a synoptic disturbance (TROUGH; TR type) shown in Figure 1.5. The synoptic-scale trough passing is expected to play an important role in moist air intrusion from outside the TP. For example, Ueno (1998) suggested evident moisture intrusion from south of the TP at a 500-hPa level for westward movement of a synoptic trough with meandering westerlies, which caused the first heavy precipitation of 1993 monsoon (Figure 1.6). Yasunari and Miwa (2006) pointed out that plateau edge cyclogenesis occurred with the enhancement of a southerly moisture inflow from the Indian plain in association with movement of large-scale westerly troughs over the TP and caused heavy rain in the Yangtze River basin. According to the stable isotope observations in August 2004, WV originated from remote areas, not from a local source, contributed to occurring precipitation with a passing trough case (Kurita and Yamda, 2008, Figure 1.7). We need to reveal impact of phase changing of Indian monsoon to the sub-continental-scale WV pathway and the linkage between the trough passage and Indian monsoon activity.

Another important factor affecting WV transportation into the TP is the effect of the Himalayas, which usually prevent the dynamic intrusion of WV into higher elevations. Local circulation with a strong daytime wind speed has been observed along deep valleys in the Himalayas (Ohata et al, 1981; Bollasina et al., 2002; Ueno et al., 2008). Inoue (1976) observed an increase in relative humidity with daytime valley winds. A weak southerly wind continues

during the night in the monsoon season, which accompanies nocturnal precipitation at the foot and in the valley of the Himalayas (Barros et al., 2000; Ohsawa et al., 2001; Ueno et al., 2001b; Bollasina et al., 2002). Barros and Lang (2003) proposed a mechanism of nocturnal precipitation by a weakening of the nighttime valley wind, stagnating the WV in front of the Himalayas. Sasaki et al. (2003) conducted numerical experiments to reveal the WV transport process over the south of TP during the post-monsoon season (October in 2000), and they showed that WV penetrated some cols of the Himalayas associated with a diurnal variation caused by a heating contrast between the TP and the Hindustan plain. At the same time, local circulation functioned to redistribute the precipitable water between the mountain and valley when there were weak general flows over the TP (Takagi et al., 2000; Kuwagata et al., 2001). For a prevailing mid-latitude trough, the contribution of such topography-influenced local circulation to diurnal changes of WV distribution should be examined.

1.4 Impact of low-level convergence and land-surface condition on cloud convections

Active cloud convection occurs after WV intrusion into the TP, and sometimes organized cloud convection was formed, as described in section 1.2. Formation process of MCS over the TP is an interest topic for many researchers, especially in terms of downstream weather modification. In the central United States, previous studies have identified several key processes for the formation of MCSs, such as low-level convergence between warm-moist southerlies and cold-dry northerlies corresponding with the passage of a synoptic trough or cold

front (e.g., Fankhauser, 1974; Ogura and Chen, 1977; Koch, 1984), enhancement of the low-level convergences caused by cloud convection (Ross, 1987), or occurrence of convective instability and forced ascending by the intrusion of a southerly low-level jet into an air mass with low equivalent potential temperature (Moore et al., 2003). Near the coastline of northwestern South America, the MCSs were triggered by low-level convergence in local circulation between the coastal areas and the Andes mountains (Warner et al., 2003). MCS propagation toward the ocean during midnight through early the next morning was induced by a gravity wave radiated from a diurnally oscillating heat source of the daytime mixed layer, which was raised up into the stratified layers of the atmosphere by the elevated terrain (Mapes et al., 2003). These studies suggested that the low-level convergence induced by the synoptic disturbance or diurnal local-circulation could strongly contribute to the MCS formation.

Over the TP, the occurrence of a “low vortex” with a diameter of about 400-800 km at the western and central plateau had been emphasized to be a key plateau-scale disturbance after the monsoon onset on the TP in 1980s (Tao and Ding, 1981; Zhang et al., 1988, Figure 1.8). The generation process of the low vortex was explained by strong land-surface heating over the western TP with the dry land-surface condition and the formation of a shear line between the southwesterlies prevailing over the southwestern part and the northeasterlies with anticyclonic circulation over the northern part of the plateau. Recently, case studies by Zhu and Chen (2003a; 2003b) attributed the MCS formation to the convective available potential energy (CAPE) due to strong land-surface thermal forcing or baroclinic instability caused by the approach of a synoptic trough, according to radiosonde sounding data the 3-demensional

numerical simulation. However, the major distributions of the low vortex do not correspond to the maximum areas of the occurrence frequency of MCSs, such as those in Li et al. (2008) shown in Fig. 1.4, and also differ from the distributions of precipitation identified by modern satellite images. One of the reasons for the discrepancies between the appearance of the low vortex and mesoscale disturbances with precipitation may be differences in the basement data, for example, many previous studies were based on the objective analysis data or model outputs with coarse resolution. There would be another fundamental mechanism of disturbances formation within the plateau affected by the vorticity-dependent low-level convergences that can be diagnosed by modern fine-mesh numerical simulations coupled with satellite data analysis.

In semi-arid regions, the soil moisture distribution is another important factor to control the formation of convective clouds or MCSs. Active convective clouds occurred in conjunction with the advection of high equivalent potential temperature (Segal et al., 1989) or low-level convergence (Cheng and Cotton, 2004), due to changes in the land-surface wetness as a result of irrigation. A sensitivity experiment changing from the Great Plains of the United States to homogeneous landscape with short glasses indicated that a thunderstorm was formed in association with the increase of convective instability due to the moistening of the near land-surface atmosphere with active transpiration from cropland (Peilke et al., 1997). In the Sahel, heterogeneity in the distribution of MCS precipitation was enhanced by partial moistening of the planetary boundary layer and strengthening of the convective instability because of land-surface wet patches caused by prior convective precipitation (Taylor et al., 1997; Taylor et al., 1998; Taylor et al., 2007; Gantner and Kalthoff, 2009, Figure 1.9). Over the TP, there is a

large decreasing trend in the surface moisture from the southeast to the northwest, causing a drastic change in the Bowen ratio of the surface flux (Xu and Haginoya, 2001; Xu et al., 2005). Accordingly, a thermally induced low-pressure system during the warm seasons prevailed in the western and central TP (Ye, 1981; Gao et al., 1981). In the east, the cloud structure is characterized by changes in the land-surface wetness. Yamada and Uyeda (2006) and Yamada (2008) pointed out that moistening of the land surface due to activation of vegetation throughout the monsoon season could reduce the evaporation of rain drops and be lower the cloud base that increased the precipitation amount under conditions of a dominant Tibetan High (Figure 1.10). Therefore, the land-surface moisture variability is a critical issue to determine the MCS genesis over the eastern plateau.

1.5 Purpose of this study

As described above sections, I need to clarify two issues for convective activity over the plateau; one is relation among Indian monsoon activity, mid-latitude wave activity, and diurnal variation of local circulation in the complex topography, which controlled the WV intrusion into the semi-arid TP, and other is land-surface heating impact to the MCSs formation over the eastern plateau. Then, the aims of this study are 1) to reveal when and how WV is transported to the TP with a prevailing synoptic-scale trough, and 2) to examine the thermally induced low-level convergence associated with plateau-scale gradient of the land-surface wetness, and their contribution to the MCSs formation over the eastern TP.

For the investigation of WV transport, first, the difference of WV advections over the

TP between the two different synoptic conditions (TR and UH type) was clarified using reanalysis data. Second, the flow pattern of WV south of and over the TP was identified, and the relation between the intraseasonal variability of the synoptic condition and the transport pathway was clarified. Finally, I carried out numerical simulations to understand temporal changes in WV transport around the Himalayas and over the TP in a typical case of the passing of a synoptic trough.

On the other hand, the formation processes of MCS over the eastern plateau are examined focusing on two factors; 1) the diurnal scale development of low-level convergences and their propagation, and 2) the contribution of surface wetness distribution for the MCS genesis. In order to identify the location of disturbances qualitatively, reanalysis data and hourly geostationary satellite IR data were used. Composite analysis was performed for development cases of large MCSs to capture the characteristics of synoptic conditions. Then, the diurnal formation processes of MCS were diagnosed using a fine-mesh numerical model.

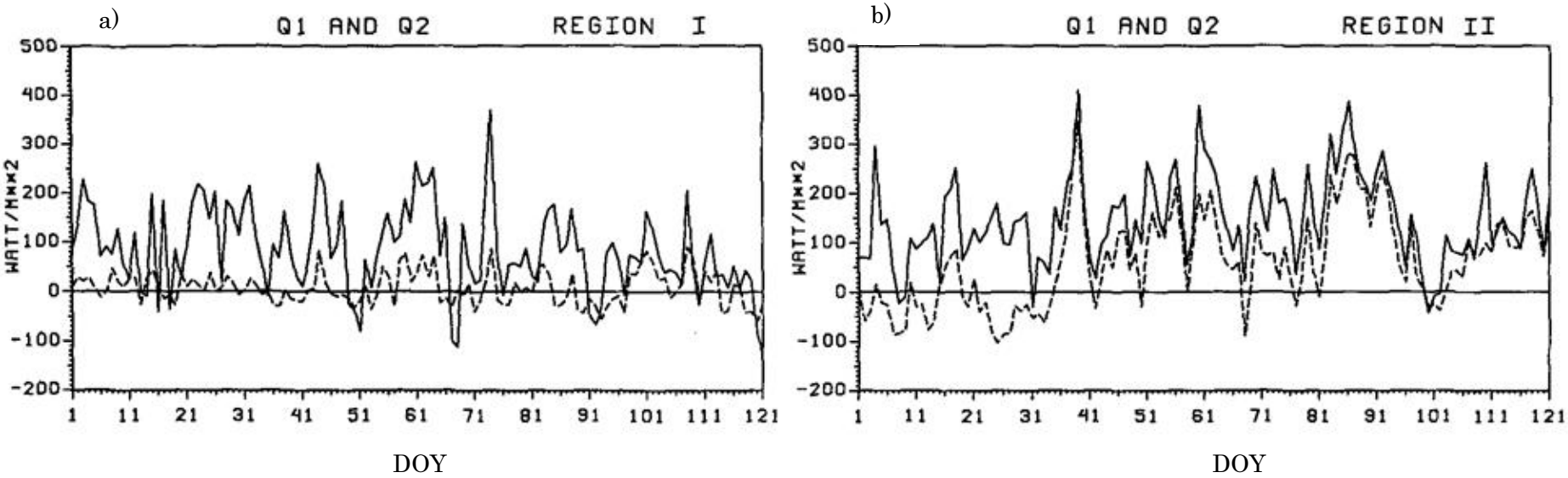

Figure 1.1. Time series of the areally averaged and vertically integrated heat source <Q1> (solid) and moisture sink <Q2> (dashed) (Wm^{-2}) for a) western plateau (REGION Ⅰ) and b) eastern plateau (REGION Ⅱ). (Yanai and Li, 1994)

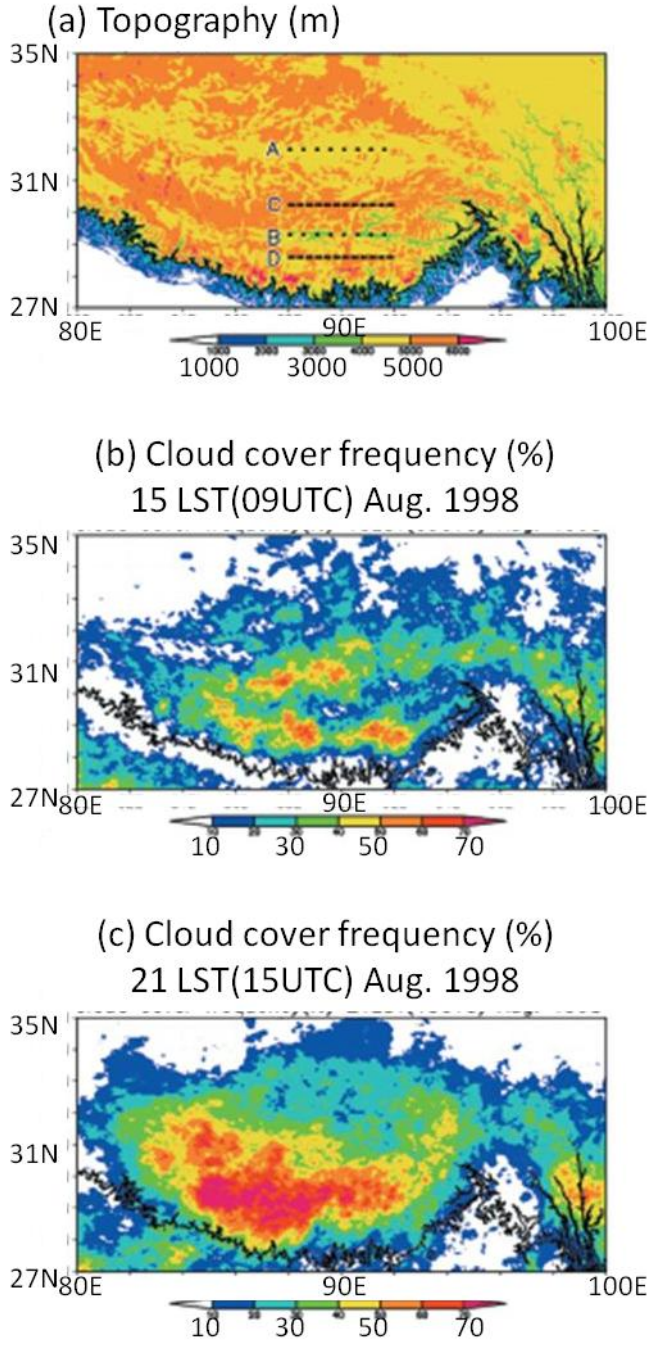

Figure 1.2. a) Tibetan Plateau topography. The solid line is the 3000 m topographic contour. Dotted lines indicate major valleys A (unnamed) and B (Yarlung-Zangbo River). Dashed lines indicate major mountain ranges C (including Nyainqentanglha Range) and D (northern part of the Himalayas). b) Average distribution of cloud-cover frequency at 15 LST for August 1998. c) As in b) but for 21 LST. (Fujinami et al., 2005)

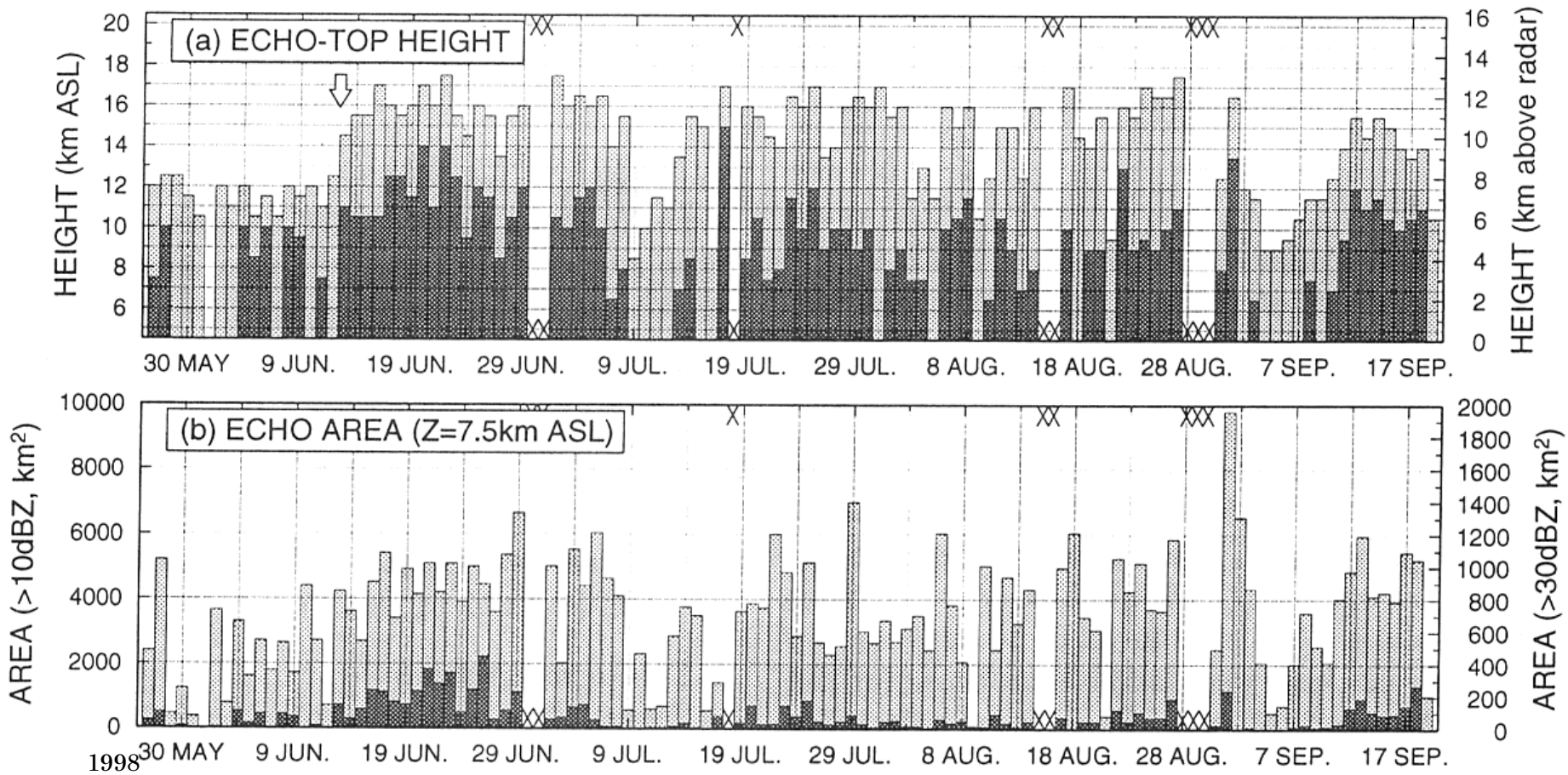

Figure 1.3. Time series of a) the maximum echo-top height obtained from the volume data of radar reflectivity and b) the echo area at 7.5 km a.s.l (3.0 km above radar level) from 27 May ro 19 September. The threshould reflectivity is 10 dBZ (light shaded area) and 30 dBZ (dark shaded area). Open arrow indicates the onset day of the Tibetan Monsoon identified by the radar observation. Cross marks indicate the missing data. (Uyeda et al., 2001)

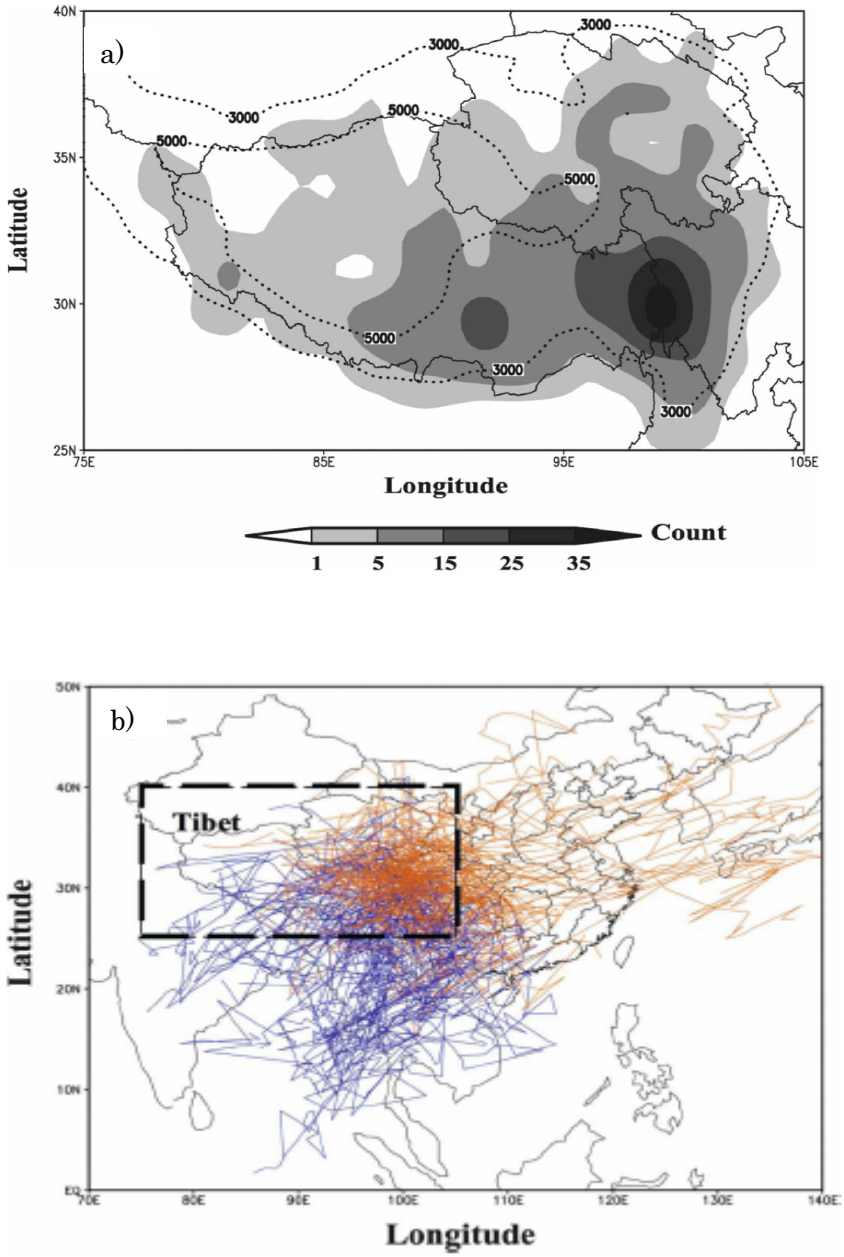

Figure 1.4. a) Spatial distribution on a 1.5 degree x 1.5 degree grid of Tibetan cloud systems initiations based on four summers (1998-2001). The dotted contours show the topography at 3000 and 5000 m. b) Trajectories of summer Tibetan cloud systems moving out of the region in 1998-2001. The blue lines mark cloud systems propagationg southward while the orange lines mark cloud systems moving out in an easterly direction. The dashed box is the selected Tibetan region. (Li et al., 2008)

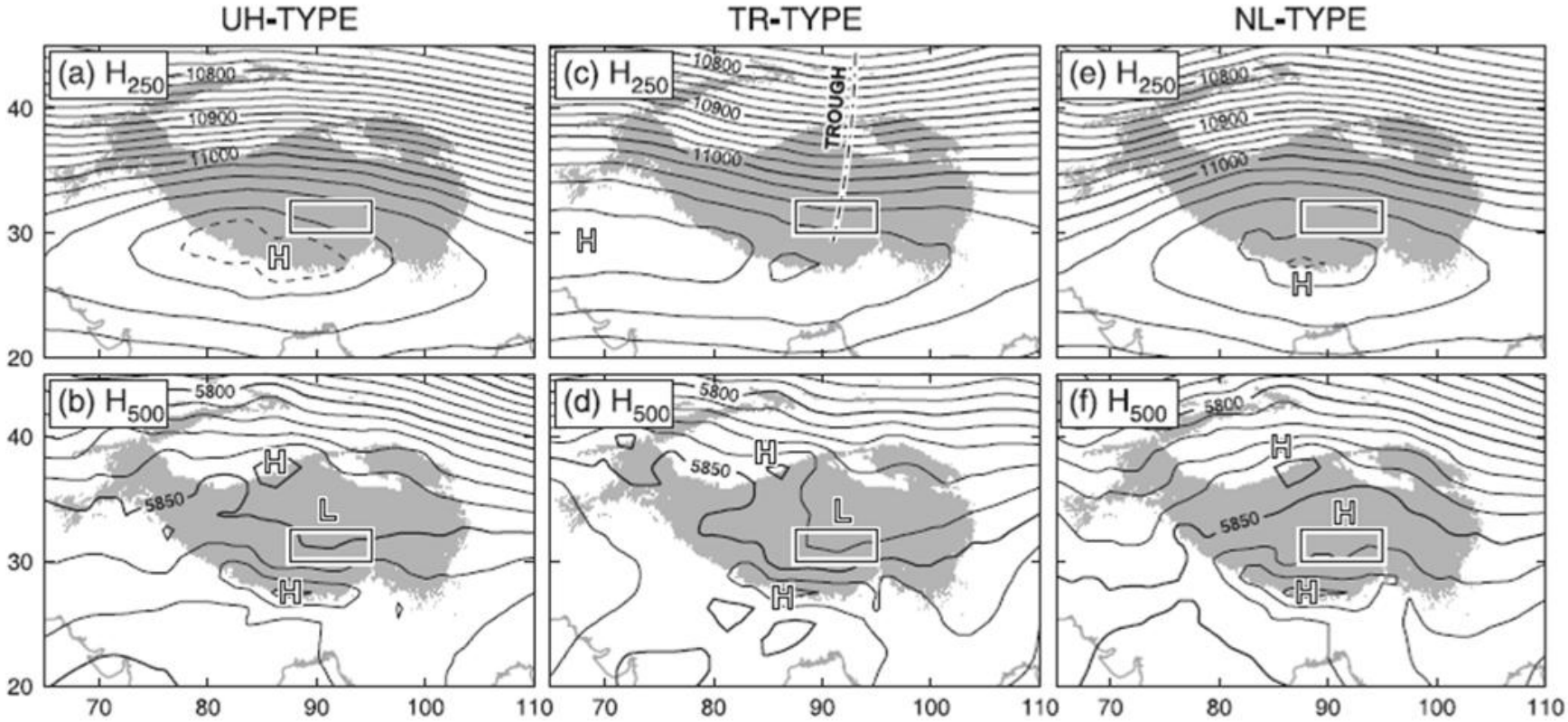

Figure 1.5. Composite horizontal distributions of 250-hPa geopotential height for three, such as a) Upper High; UH, c) Trough; TR, and e) No Low; NL types, respectively. The contour interval is 20 gpm, and an additional contour of 11090 gpm is drawn by a dashed line. Figure b), d), and f) are same but at 500 hPa. The contour interval is 10 gpm. (Yamada and Uyeda, 2006)

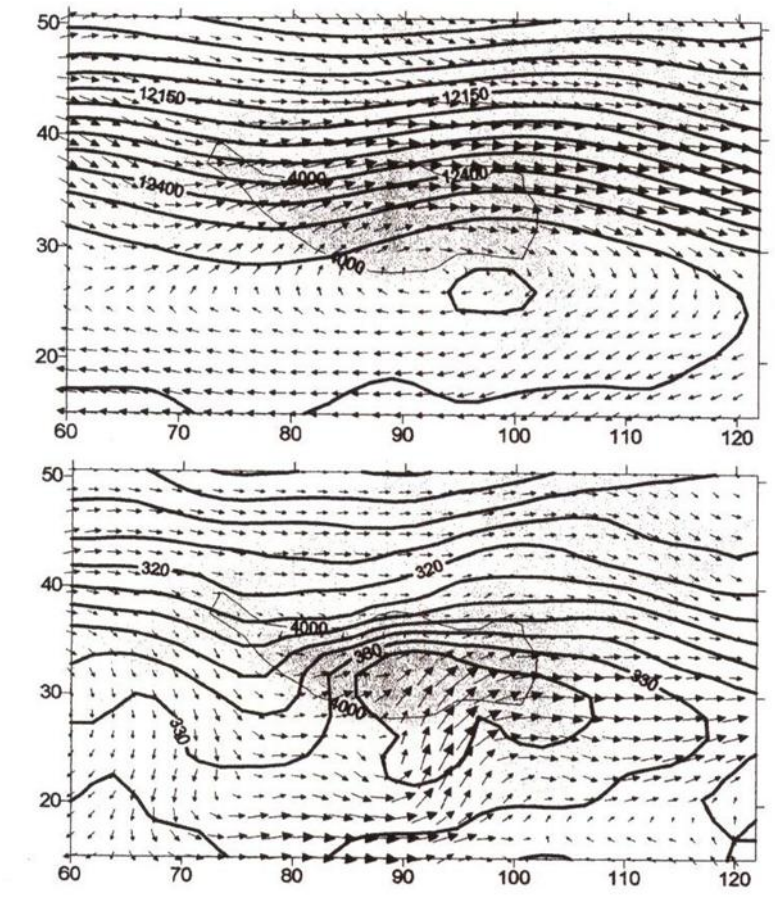

Figure 1.6. Averaged pressure and wind distribution at 200 hPa (upper), and averaged qV vector with potential temperature (solid line) distribution at 500 hPa (lower), from June 16 to 20, 1993. Topography of the plateau used for calculating GANAL data is shown as hatched pattern. (Ueno, 1998)

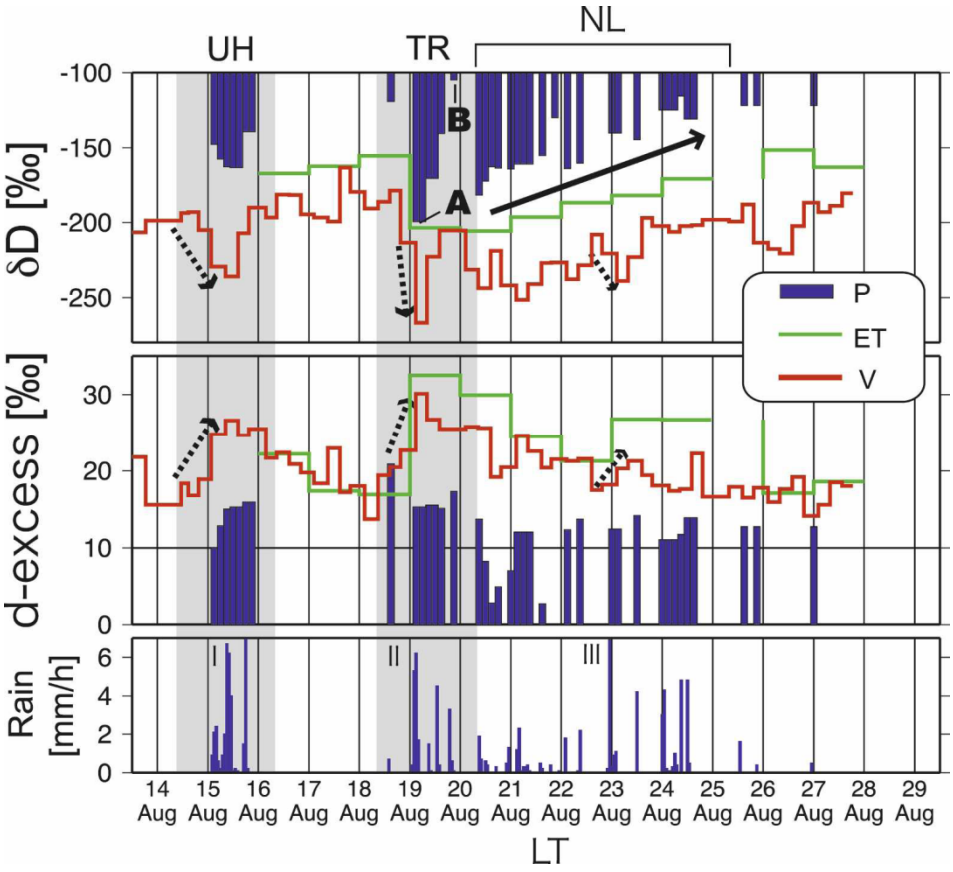

Figure 1.7. Time series of (top) δD and and (middle) d excess in precipitation (P; blue bar) atmospheric moisture (V; red line), and (bottom) daily average evapotranspiration (ET; green line) and rainfall intensity at the observation site during the intensive observation period. UH, TR, and NL show synoptic condition pattern described in Figure 1.5. A and B indicate rainfall events when the TR-type precipitation started and ended. The arrows with a broken line represent the isotopic changes in atmospheric moisture when intense rainfall (5 mm h-1) was observed (labeled Ⅰ, Ⅱ, and Ⅲ). The arrow with a solid line shows the tendency of the isotopic evolution of the δD value during the NL-type rainfall period. (Kurita and Yamada, 2008)

a)

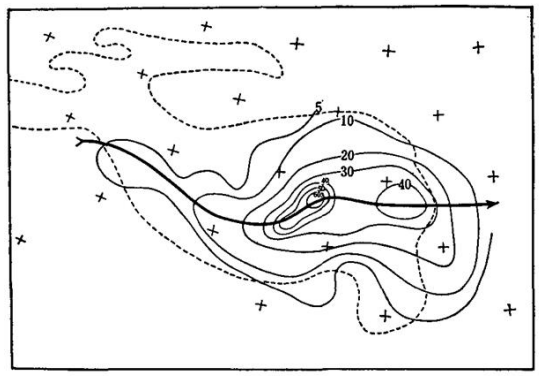

b)

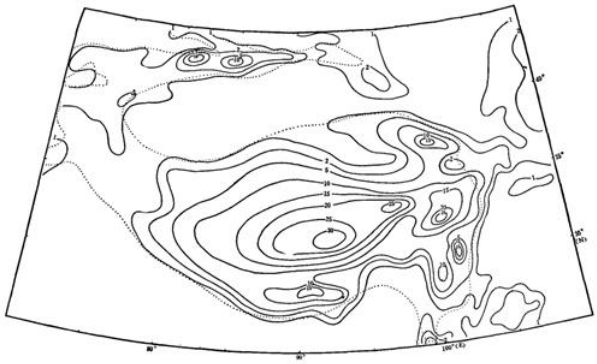

Figure 1.8. a) The frequency distribution of low-level vortices over the plateau during the period May-September 1969-1976. b) Distribution of the annual mean number of days of occurrence of hailfall over the plateau and its surroundings. (Tao and Ding, 1981)

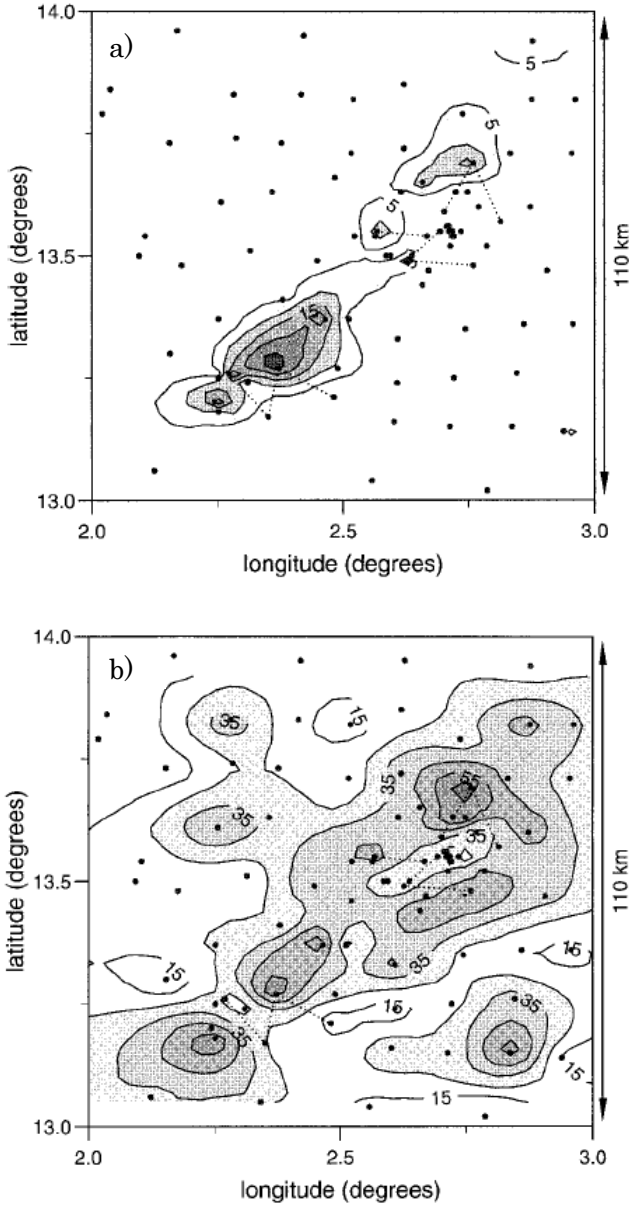

Figure 1.9. Daily rainfall (mm) on a) 20 and b) 22 July 1992. Pairs of gauges used in the regression are joined by dotted lines. (Taylor and Level, 1998)

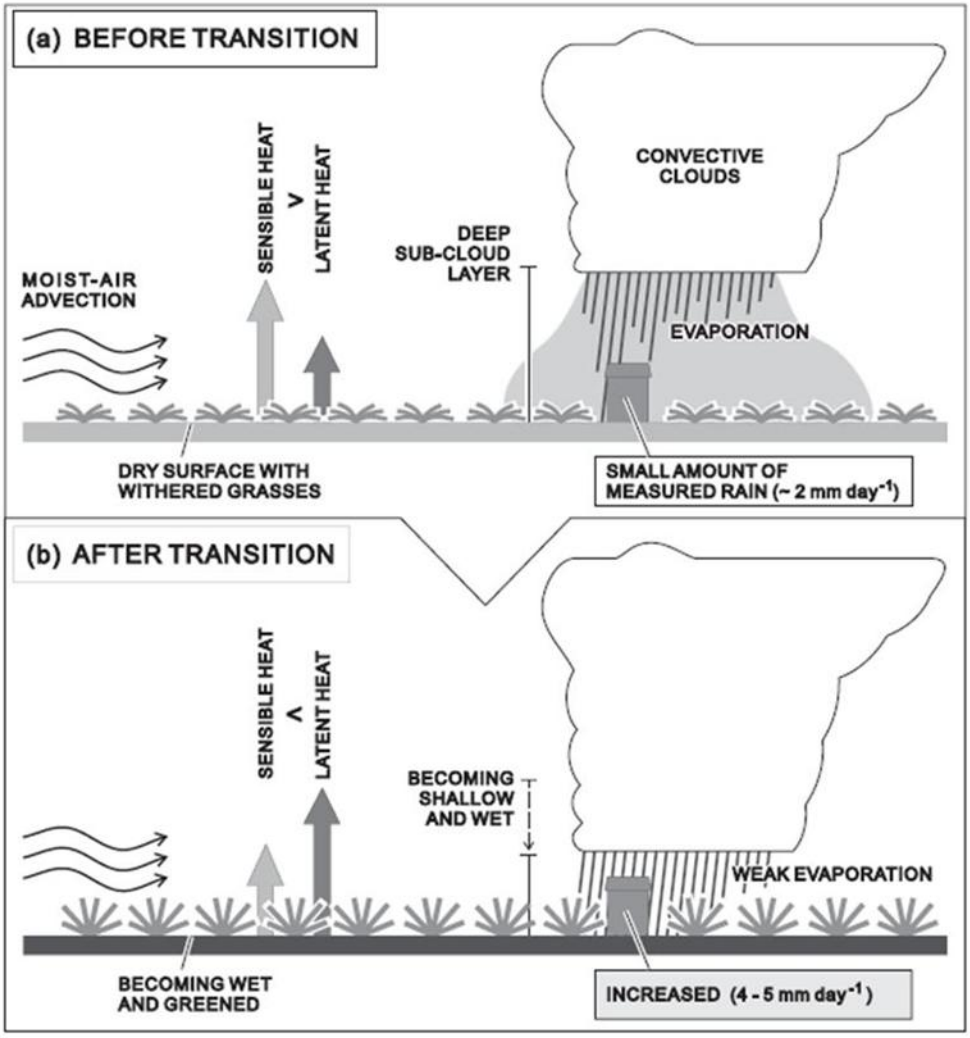

Figure 1.10. Schematic illustration showing the transition of the rainfall characteristics in a UH type rain event due to changes in the ground conditions. (Yamada and Uyeda, 2006)

Chapter 2 Data and Methods

2.1 Reanalysis data

WV transport process was analyzed in the mature monsoon season (from July to August) of 1998 using GAME reanalysis data (Yamazaki et al., 2003). This reanalysis data was generated by assimilating the observed data, including more than 100 sonde sites and wind profiler sites. The highest horizontal resolution of released data was 0.5 degrees in the Asian monsoon region. Horizontal resolution of topography using assimilation was 0.5625 degrees. On the other hand, JRA25 with 1.25 degree grid-spacing (Onogi et al., 2007) was used for the analysis of the MCSs formation in 1998-2006, because GAME reanalysis data was constructed only from April to October in 1998.

2.2 Extraction of analysis cases of UH and TR types in 1998

For the WV transport analysis, dominant cases were selected on the GAME reanalysis field in order to investigate large-scale circulation focusing on the differences between the UH and TR type. The TR type was specified according to two criteria: 1) the geopotential height at 500 hPa, averaged over an area of 30-40°N and 85-95°E, decreased more than 20 m with a minimum height of less than 5860 m, and 2) a trough was recognized over the TP in the 500 hPa synoptic chart. The UH type stipulated that the 200 hPa geopotential height averaged over an area of 30-40°N and 85-95°E reached more than 12615 m for three consecutive days. Accordingly, five or four cases which included a total of 10 or 16 days were chosen for TR or UH types, respectively (Table 2.1a). Almost all of the selected cases were the same as the UH and TR, as

classified by Yamada and Uyeda (2006).

2.3 MCS extraction and tracking

The behavior of MCS on the TP was examined in the mature monsoon season (from July through August) during 1998-2006. TP areas are defined as those more than 3500 m above sea level (a.s.l.) in the domain of 29-40N, 70-103E, where MCSs are extracted using hourly IR data observed by the Meteosat-5 (conduct level 1.5) geostationary satellite located over the Indian Ocean at 0 N, 63 E. Original satellite images are composed by perspective projection with inhomogeneous latitude/longitude intervals in the range of 5-10 km spatial resolution. Data were re-sampled with 0.15 (about 15 km) grid spacing after transformation to brightness temperature (Tbb) using a conversion table.

Methods of MCS extraction and tracking conformed to Evans and Shemo (1996), and it has been applicable in the Himalayas and TP region by the Barros et al. (2004). First, a continuous area larger than 4000 km^2 and with Tbb less than 219 K (hereafter, the target cloud area) was identified. The Tbb threshold with 219 K is appropriate over the plateau, because Uyeda et al. (2001) pointed out that echo top of convective precipitation observed by Doppler radar in the central TP reached to 17 km above sea level. If grids with Tbb less than 235 K existed around the target cloud area, the grids were treated as candidate areas of MCS. This requirement allows the criteria of cumulus convections with precipitation. Next, target cloud areas at time t were compared with the image of one hour later (t+1). If they overlapped more than 40 % (or greater than 10^4 km^2), they were categorized as the same target cloud area, and

target clouds tracked for more than 6 hours were determined as MCSs. If two target cloud areas merged, the larger one was chosen for continued tracking, and the smaller one was terminated. In this study, a grid with minimum Tbb was identified as the location of MCS and tracked to calculate the MCS movement. If one snapshot of the original Metoesat5-IR image was missing, the Tbb fields were interpolated on the time sequence, and MCS tracking was continued. If the image continued to be missing for more than 2 hours, tracking of MCS was stopped at the time in which the image started to fail, and extraction was restarted at next 00 UTC (i.e., 06 local time; LT calculated along 90E).

After the MCS tracking, the initial and extinct location/time, continuance, maximal area, max time, and migration length were calculated. Continuance means the time from the occurrence of the MCSs to their extinction. Max time was defined the time when the MCSs reached the maximal area. Migration length indicates the distance from the initial to the extinct location.

2.4 Numerical design of Non-Hydrostatic Model (NHM) for WV transportation analysis

In order to diagnose WV transport process from southern foot of Himalayas to the TP, I conducted a numerical simulation for all TR type cases in 1998 (Table 2.1b). From this numerical experiment, the WV transport process with temporal variations from the foot of the Himalayas to the TP was identified. NHM developed by the Meteorological Research Institute and the Numerical Prediction Division of the Japan Meteorological Agency was used in this

study. The fundamental equations are three-dimensional, non-hydrostatic and full compressional. The bulk method including the cold rain process was chosen for cloud microphysics (Ikawa and Saito, 1991). In this method, the water substance is classified into six components (water vapor, cloud water, cloud ice, rain, snow, and graupel), and the mixing ratio of each component is calculated. The transformation process of water, including graupel, is important for simulating the precipitation process because, as indicated by Uyeda et al. (2001), the formation of graupel particles is a characteristics of convective clouds over the southeastern TP. The Kain and Fritsch scheme (Kain and Fritsch, 1990), which is suitable for calculating cumulus convection at middle latitudes, was used. The evapotranspiration efficiency and albedo are 0.3 and 0.2 for land and 1.0 and 0.6 for ocean grids, respectively. The GAME reanalysis data with a grid spacing of 0.5 were used for the initial and boundary conditions. The calculation was started 12 to 24 hours prior to each analysis period for spinup. The vertical coordinate was the Z*-coordinate with an unequal grid interval. The minimum layer depth was 40 m at the lower layer, and the maximum layer depth was 1200 m in the upper layers. The horizontal resolutions for a coarse domain and a nesting domain were 30 km and 6 km, respectively. The 30-km grid spacing was nested in the GAME reanalysis data every 6 hours, followed by 6 km grid spacing nested in the 30 km simulation every 3 hours by a one-way nesting scheme. An interpolated topography data set in each grid size extracted from GTOPO30, which obtained from United States Geological Survey, was used in the model. Topographic features of the numerical domains are shown in Fig. 2.1. In the first domain, with 30-km grid spacing, the Tanggula and Nyainqentanglha mountains are recognized (Fig. 2.1a).

The complex topographic features in the TP and major valleys transecting the Himalayas can be recognized only in the second domain, with 6-km grid spacing (Fig. 2.1b). Both domains were set as large as possible for computational efficiency.

2.5 Numerical design of Weather Research and Forecasting (WRF) model for MCSs formation analysis

In order to investigate plateau-scale behavior of low vortex and formation mechanism of low-level convergence causing the MCS occurrence, numerical experiment was carried out for three typical cases. Selected reason of target periods is explained in Section 4.2. The WRF model, Ver. 3.0.1.1 (Skamarock et al., 2008), was used. One calculation period covers 120 hours, including one day for a model spin-up (Table 2.2). Interpolated topography data was obtained from GTOPO 30 data constructed by the United States Geological Survey. Two simulated domains were set, i.e., Domain 1 covering 12.5-50N, 55-115E with 60 km grid spacing and Domain 2 covering 18-46N, 63-110E with 20 km grid spacing (Figure 2.2a). Large-scale mountain ranges in the plateau, such as Tanggula and Nyainqentanglha, were described in the calculation domain 2. The vertical coordinate was the σ–coordinate with 31 layers, and the top layer was 50 hPa.

Fundamental equations were constructed using three-dimensional, non-hydrostatic, and full compressible. WRF Single Moment (WSM) 6 Scheme (Hong and Lim, 2006) of the bulk method was chosen for the cloud microphysics. In this scheme, water was classified into six components (water vapor, cloud water, cloud ice, rain, snow, and graupel), and the mixing ratio

of each component was calculated. For the cumulus convection scheme, the Kain and Fritsch scheme (Kain and Fritsch, 1990) was used because it was suitable for calculating the cumulus convection at the mid-latitudes. Land component parameters, such as the albedo, soil moisture, sensible and latent heat fluxes, and soil temperature, were calculated by the Noah land-surface scheme (Chen et al., 1996; Chen and Dudhia, 2001; Ek et al., 2003), which could reproduce soil temperature and surface fluxes at the central Tibetan Plateau (e.g. Velde et al., 2009).

JRA-25 was used for the atmospheric initial and boundary conditions for the simulation. The atmospheric boundary condition was nested every 6 hours. The initial land condition, except for the soil moisture, was produced from JRA-25 by interpolating the original 2.5 grid spacing to 1.25 grid spacing. For the soil moisture, Aqua/AMSR-E Level 3 standard product Version 5.0 (Koike et al., 2004) was averaged from July through August during 2002-2006 and adopted as the initial condition. The soil moisture distribution is shown in Figure 2.2b, indicating a drastic decrease from the southeast to the northwest in the plateau with wet zones along the southern foot of the Himalayas and east of the TP. The Noah land-surface scheme did not require a boundary condition of all physical components of land, including the soil moisture.

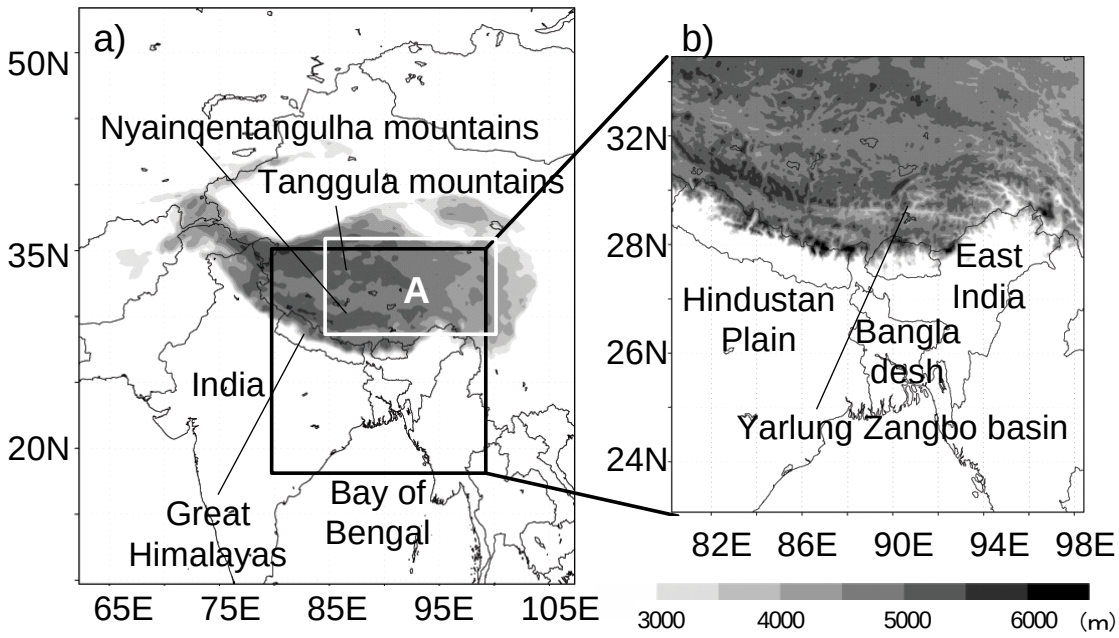

Fig. 2.1 a) First domain and b) second domain of the NHM simulation over 3000 m a.s.l. (shaded). White box (A) indicates the analysis area of WV advection, as explained in Section 3.1.

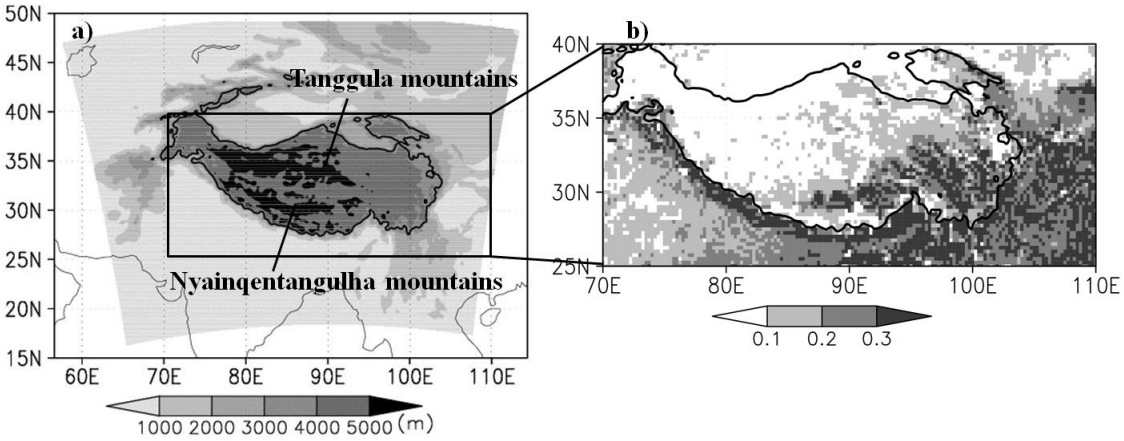

Figure 2.2 a) Topography around the Tibetan Plateau. The shaded area is the second domain of the numerical simulation. The solid line shows the topography at 3500 m. b) Orginal soil moisture distribution of AMSR-E averaged from July to August 2002-2006.

Table 2.1　a) Analysis periods for the cases of the TR and UH types during the 1998 monsoon.　b) Periods of NHM simulation for the TR type.

a)

	TR type	UH type
Case 1	18 UTC, July 6 – 18 UTC, July8	18 UTC, July 1 – 18 UTC, July 4
Case 2	18 UTC, July 23 – 18 UTC, July 25	18 UTC, July 17 – 18 UTC, July 19
Case 3	18 UTC, August 2 – 18 UTC, August 4	18 UTC, July 26 – 18 UTC, August 2
Case 4	18 UTC, August 11 – 18 UTC, August 13	18 UTC, August 5 – 18 UTC, August 9
Case 5	18 UTC, August 16 – 18 UTC, August 18	

b)

	Calculated periods
Case 1	18 UTC, July 3 – 06 UTC, July 10
Case 2	06 UTC, July 23 – 06 UTC, July 27
Case 3	18 UTC, August 1 – 06 UTC, August 6
Case 4	18 UTC, August 10 – 06 UTC, August 15
Case 5	18 UTC, August 15 – 06 UTC, August 20

Table 2.2 Periods for three numerical simulation cases of MCSs formation study.

Target day	Caluculated preriod
Jul. 4, 1998	00 UTC Jun. 30 – 00 UTC Jul. 05 in 1998
Jul. 2, 2001	00 UTC Jun. 28 – 00 UTC Jul. 03 in 2001
Aug. 26, 2005	00 UTC Aug. 22 – 00 UTC Aug. 27 in 2005

Chapter 3 Transport process of WV into the TP

3.1 Relation between monsoon circulation and WV intrusion

WV transportation from the Indian Ocean to the plateau is expected to be affected by sub-continental scale changes in Indian monsoon flows. A relation between the WV transport pathway in south-east Asia, including the TP, and the intraseasonal variability of the Indian monsoon was revealed by Sugimoto et al. (2008). First, horizontal WV advection was calculated for Upper High (UH) and Trough (TR) types in the domain of 28-35.5°N, 85-100°E (A in Fig. 2.1) and compared with the WV advection from different directions (Fig. 3.1). The WV inflow from each direction was integrated between 500 and 300 hPa in the GAME reanalysis data. A daily average WV budget of 1.9×10^{12} kg/day converged in the case of the TR type. Meanwhile, the convergence amount for the UH type was nearly 0 kg/day, meaning that a large amount of WV intrusion from outside occurred for the TR type. For both types, about 2.5×10^{12} kg of WV per day came in from the western boarder while about 3.9×10^{12} kg WV went out to the eastern boarder, including that there was little convergence of WV along the east-west direction over the TP. On the other hand, the southerly advection was larger for the TR type and accounted for about 60 % of the total inflow from all directions. The combined evidence indicated that the intrusion of WV into the TP from the south dominated for the TR type but not the UH type.

Next, in order to identify the main pathway of WV transport over the south of the TP, WV flux and geopotential height at the lower (850 hPa) and middle (500 hPa) troposphere were compared for the two types (Fig. 3.2 and Fig. 3.3). At 850 hPa (Fig. 3.2), the distributions of

geopotential height differed over the Indian subcontinent. In the case of the UH type, a monsoon trough expanded southward over north India (α in Fig. 3.2a), and a large latitudinal pressure gradient occurred over southern India with an intensification of the monsoon westerlies (shown as larger vectors in Fig 3.2b). The route of westerlies changed towards the north with cyclonic rotation over the northern BoB. Part of this northerly flow intruded westward along the monsoon trough extending in front of the Himalayas. In contrast, the low-pressure zone over the northwest of India (α) shrank in the case of the TR type (Fig. 3.2c), with a shift in the flow axis north toward the foot of the Himalayas (Fig. 3.2d). Accordingly, the main monsoon westerly channel passed over the central Indian subcontinent from the Arabian Sea to reach the Himalayan ranges directly. The pathway of the TR type obviously differed from the low-level flow patterns generally recognized in the monsoon season (e.g. Kesshavamurty and Awade, 1970; Fujinami and Yasunari, 2004) that indicating prevailing southeasterly flows from the BoB to the TP, as shown in Fig. 3.2b. In other words, the UH type flows represent the features of averaged Indian monsoon flows. Murakami (1976) revealed an intraseasonal oscillation of the Indian monsoon on a 15-day time scale that accompanied the north (south) shift of monsoon westerly in the break (active) phase. Precipitation in northern India increases during the break phase of the monsoon in central India (i.e. Kurishnamurthy and Shukla, 2000; Goswami and Mohan, 2001). Murakami (1986) also pointed out that the precipitation amount at the foot of the Himalayas had an inverse correlation with the precipitation amount in central India because of a change in the WV pathway with the oscillation of monsoon westerlies. The daily average precipitation amount, analyzed using Global Precipitation Climatology Project (GPCP) data,

over the southern foot of Himalayas in the present case of the TR type was larger than in the case of the UH type (figures are omitted). Accordingly, the differences between the UH and TR types in terms of the sub-continental-scale flow patterns with latitudinal shifting of the major WV transportation paths under synoptic-scale conditions correspond to the changing phases of the Indian monsoon.

The vertical distributions of specific humidity and flux along the main westerlies in the case of the UH and TR types (transect A-B-C and D-E-F in Fig. 3.2b and Fig. 3.2 d) are compared in Fig. 3.4. The distribution of specific humidity showed a similar structure in both types. For example, there was a decrease in WV with an increase in height (Fig. 3.4a and 3.4c), and the main flow of WV was below 700 hPa (Fig. 3.4b and 3.4d). However, the flux near the southern slope of the Himalayas differed between the two types. The amount of WV intrusion over the TP was larger in the case of the TR, corresponding to Fig.3.1. A larger WV flux appeared from Bangladesh toward the southeastern TP at 500 hPa in the case of the TR type. This difference was also recognized in the flux distribution of 500 hPa (Fig. 3.3b and 3.3d). In the geopotential height fields of the mid-troposphere for the UH type (Fig. 3.3a), a low-pressure area existed with its center at 18°N80°E. A cyclonic flow associated with this low-pressure area played an important function in changing the WV from the BoB westward before reaching to the TP. It moved to the Arabian Sea, passing over northern India (Fig. 3.3b). Mujumdar et al. (2005) identified a similar cyclonic circulation over India in the middle troposphere during the active phase of the Indian monsoon. Therefore, the appearance of a low-pressure area in the case of the UH type is quite reasonable in the active monsoon phase in India. The formation

mechanism of the low pressure is the southward tilting of a low-level monsoon trough with an increase in altitude (Rao and Ramamurthy, 1968) or a cut-off low after passing a trough at 500 hPa by the dynamic effect of TP (Yanai and Wu, 2006). In the case of TR type, the low-pressure area disappeared over India at 500 hPa (Fig. 3.3c), and weak westerlies prevailed there (Fig. 3.3d). A strong southwesterly flux corresponding to the front of synoptic trough expanding around 25-32°N, 90-100°E also appeared over Bangladesh (Fig. 3.3c).

Consequently, differences between the UH and TR type in terms of the large scale circulation in the south of the TP corresponded with the active/break phase of the Indian monsoon and changed the WV flux direction at the mid-troposphere near the southern periphery of the TP through the establishment of cyclonic circulation with a low-pressure system over the Indian subcontinent, which affected the moisture budget over the southeastern TP. Results of objective-analysis data are inconclusive regarding the moisture transportation near the massive topographical features, such as the Himalayas. Mountain ranges usually induce local diurnal circulation, which plays an important role in low-level moisture transportation that is unrecognizable in the reanalysis data. In the next section, details of the WV transport process were again identified for the TR type through the use of a non-hydrostatic numerical model around the southeastern TP.

3.2 Transport process of water vapor intruding into the southeastern TP

To consider the WV transport process into the TP, I need to reveal the mechanisms of WV to crossing over the Himalayas, which usually act as a barrier to atmospheric flow. A

high resolution numerical simulation by NHM was performed for five cases of the TR type (Table 2.1b). The detail numerical design was shown in Section 2.4. In this section, the WV transport process from the lower elevations south of the Himalayas to 4000 m level over the southern TP was detailed for Case 1, when the deepest and largest trough expanded over the southern TP. Hereafter, NHM simulations are described as NHM_30 and NHM_6, with grid sizes of 30 and 6 km in different domains (see Fig. 2.1), respectively.

First, the reproducibility of synoptic and plateau-scale circulations by NHM was validated by GAME reanalysis and METEOSAT5-IR data. For all cases listed in Table.2.1b, a westerly wind accompanied by a low-level monsoon westerly over northern India and a Tibetan High centered over the western TP in the upper troposphere were simulated well in NHM_30 (figure was omitted). In Fig. 3.5a and b, GAME reanalysis and NHM_30 for July 7-8 showing geopotential height and wind vectors at 500 hPa are compared. The geopotential height distribution showed two troughs separated north-to-south around 90°E and controlled WV intrusion in the southern TP all day on 7-8 July. One of the troughs is in the north of the TP (around 45°N, 95°E; TR1), and the other is over the TP (around 30-35°N, 80-98°E; TR2). A westerly flow penetrates the two troughs along 35-40°N. Large-scale circulation patterns over the TP, represented in the GAME reanalysis, were also simulated by NHM.

On the other hand, in the case of the NHM_30, a mesoscale cyclonic circulation (Low_A) was formed at the center of the TP at 06 LT on 7 July. This Low_A migrated northeastward and reached 35°N, 100°E at 18 LT on 8 July. Westerlies along 35-40°N converged with easterlies in the northern part of TR2 (Line_B). A similar circulation and low-pressure

system with a convergence line were recognized in four other TR cases by NHM simulations. Cloud areas in the METEOSAT-5 IR images (Fig. 3.5c) were compared with the results of NHM_30 in order to examine in detail the formation of disturbances. Over the southern and southeastern TP, a cloud area corresponding to TR2 was discernable from the afternoon into the night. Cloud convections were very active ahead of TR2, with southwesterlies crossing over the eastern Himalayas. In addition, a mesoscale convection (Cloud_A) developed in the same area of the Low_A in NHM_30. Over the western TP, a dry intrusion with cloud-free areas distributed with the forming cloud zone (Cloud_B) at a head, which was consistent with the formation of Line_B by NHM_30. This evidence confirmed that the NHM could simulate the mesoscale circulation and the convergence zones over the TP.

Temporal changes of WV distribution around the Himalayas were identified by fine-mesh simulation results (NHM_6) nested in the NHM_30. Figure 3.6 shows wind and specific humidity at three-hour intervals at 1500 m a.s.l. on two successive days (7-8 July). Moist air was flowing from the west along the foot of the Himalayas below about 2000 m a.s.l. on July 7. This flow was a part of the main monsoon westerly intruding from the Arabian Sea (shown in Fig. 3.2d). In the afternoon, specific humidity increased in wider areas, especially over Bangladesh and East India. The simulated potential temperature profile showed that the mixing layer depth over the south of the Himalayas was around 500 m in the early morning but developed to 1500 m in the afternoon (figures are omitted). Therefore, the increase in moisture could be explained by two factors: the low-level intrusion of moist air associated with monsoon westerlies and the development of a mixing layer over the land.

During the afternoon, the wind direction also changed from west to southwest over Bangladesh. As shown by latitude-height sections of wind speed along 93°E (left in Fig. 3.7), an upslope wind was simulated all day but was enhanced in the mid-afternoon in the southern slope of the Himalayas. This diurnal change of wind speed in the Himalayan slope was consistent with the findings of past observational studies (Ohata et al, 1981; Bollasina et al. 2002; Ueno et al., 2008). WV flux from the south of the Himalayas increased along with the enhancement of daytime wind speed (Fig. 3.7, right). The afternoon increase in WV flux corresponded to the findings of a past observation (Inoue, 1976). Therefore, the simulation by NHM_6 suggested that a strong daytime upslope wind near the Himalayas transported WV in the mixing layer from low elevations to high elevations over the southern TP. From midnight to the next morning, the specific humidity in the lower elevations decreased due to the disappearance of the mixing layer. A similar diurnal variation of WV distribution was repeated on July 8. Accordingly, in the NHM simulation, WV transportation in front of the Himalayas was controlled by several important systems, such as a low-level rich moisture intrusion from the west, the daytime development of a mixing layer, and a strong upslope wind intruding into the TP.

Finally, characteristics of the WV distribution over the southern TP were examined after the intrusion. Figure 3.8 shows the flux and specific humidity at 5500 m a.s.l. on 7-8 July. Areas above 5000 m a.s.l are shaded light gray. A wetter zone of more than 0.008 kg/kg (dark shaded) appeared south of 29°N at 12 LT. This zone was formed with a convergence between a wetter southwesterly wind intruding from the south of the TP and drier northwesterly winds in the rear of the trough and was consistent with an active convective zone ahead of TR2, as shown

in Fig. 3.5. The moisture zone expanded northeastward by the evening intensification of the southwesterly crossing over the Nyainqentanglha mountains (about 31°N). The wetter zone disappeared from midnight to early the next morning due to the weakening of a moist southwesterly crossing over the Himalayas. A similar moisture convergence was repeated on July 8. Using results of a numerical experiment of WV transport in October, Sasaki et al. (2003) indicated that southerly upslope winds with a moist air mass in a valley of the Himalayas intruded into the southern TP, and general westerlies over the TP formed a stationary moisture front. Although they showed only the contribution of an upslope wind for WV intrusion, our simulation results suggest that the circulation pattern associated with the synoptic trough affected the distribution of WV over the southeastern TP. Namely, WV transported from the southern foot of the Himalayas converged zonally over the southern/southeastern TP but did not expand widely into the central TP due to northwesterlies following the trough from the afternoon into the night. The effect on the WV convergence of a diurnal-induced upslope wind along the southern slope of the Himalayas and the synoptic flow pattern over the TP were systematically driven in the case of the TR type, and this WV transport process was different from the WV redistribution caused by the local circulation with mountain ranges, as explained by Takagi et al. (2000) and Kuwagata et al. (2001).

3.3 Summary for WV transport process

Many past studies have focused on the thermodynamic function of the TP with large diurnal convective activities that are usually accompanied by strong land-atmosphere

interactions under a prevailing Tibetan High. This study focused on the WV transport processes from the Indian Ocean into the TP under a prevailing of synoptic-scale trough during the 1998 monsoon season. The major results are summarized as follows.

1) According to the WV budget analysis, a large amount of WV intruded from the south and converged over the TP in cases of the TR type. WV convergence associated with horizontal advection was scarce for the UH type.

2) A composite analysis of GAME reanalysis data showed large differences in the subcontinental scale WV flow pattern between the UH and TR, corresponding with the active/break phase of Indian monsoon activity. In the case of the UH type, a moist air mass passing over the BoB in the lower layer reached to the south of the Himalayas. WV was then transported westward before reaching over the TP due to a cyclonic circulation formed over the Indian subcontinent in the mid-troposphere. On the other hand, in the case of the TR type, low-level monsoon westerlies were directed to the foot of the Himalayas passing over central and northern India that provided WV intrusion into the TP.

3) A diurnal variation in WV advection from south of the Himalayas to the southeastern TP was identified by NHM in a representative case of the TR type. The WV transport was complexly intertwined with some physical factors in the lower and middle troposphere. Then, Schematic diagrams of the transport processes are shown in Fig. 3.9. WV supplied to the south of the Himalayas by monsoon westerlies in the lower troposphere reached 1500 – 2000 m a.s.l with the development of a mixing layer in the afternoon. At the same time, upslope wind in the southern slopes of the Himalayas lifted the moist air mass to the plateau

level. Over the TP, a convergence zone of WV was formed by moist southwesterlies in front of the synoptic trough and a dry northwesterly behind it. This convergence zone expanded northward in the evening and disappeared by the next morning due to the weakening of a moist southwesterly crossing over the Himalayas. The results of the NHM simulation study suggest that WV transportation processes are composed by multiple steps.

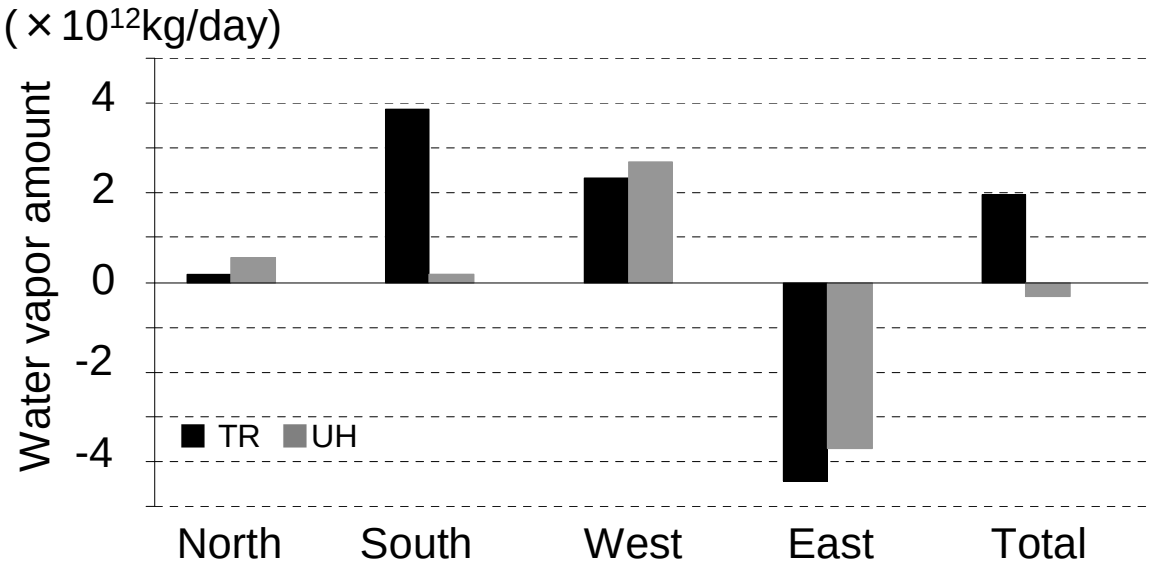

Fig. 3.1. WV budget calculated in Box A (see Fig. 2.1), in the cases of the TR (black) and UH (gray) types. Positive/negative values correspond to the inflow/outflow of WV flux.

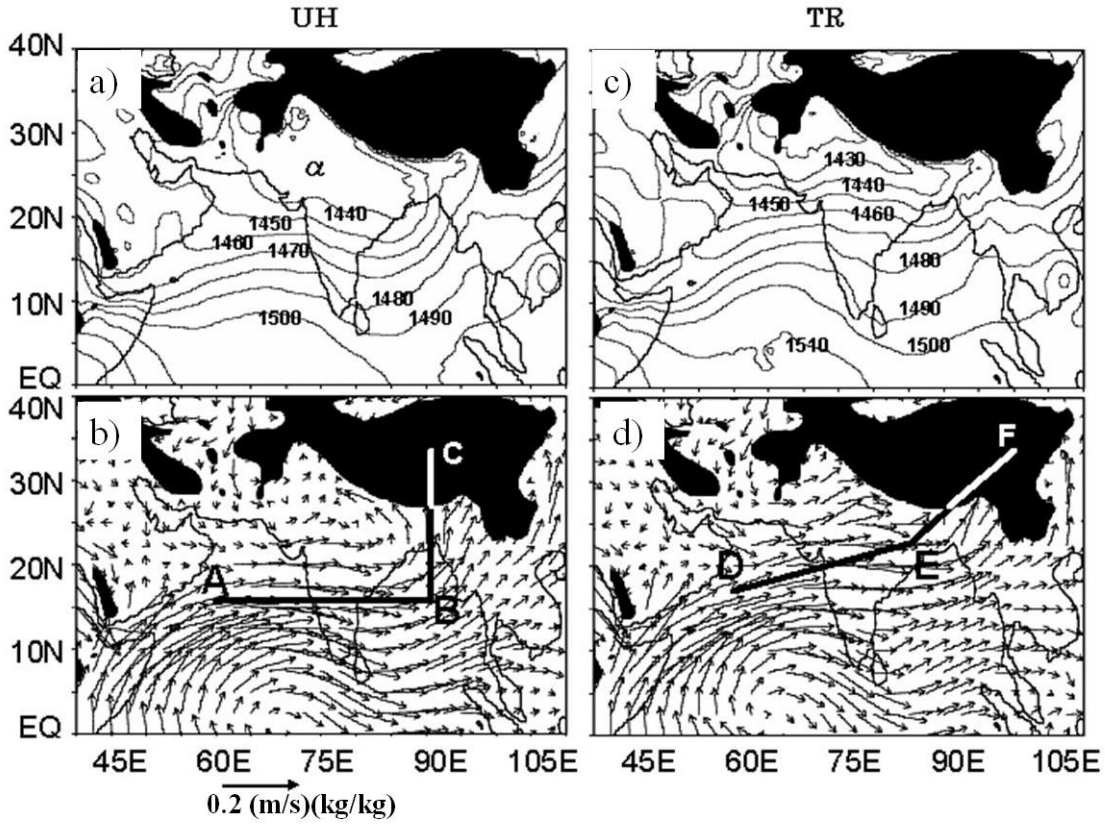

Fig. 3.2. Composites of geopotential height (unit; m) and WV flux (unit; kg/kg× m/s) at 850 hPa. Left (right) figures correspond to the UH (TR) type. Areas above 1500 m are masked out with black shading. α in a) means monsoon trough. A vertical cross-section of specific humidity and WV flux along the transections A-B-C and D-E-F is shown in Fig. 3.4.

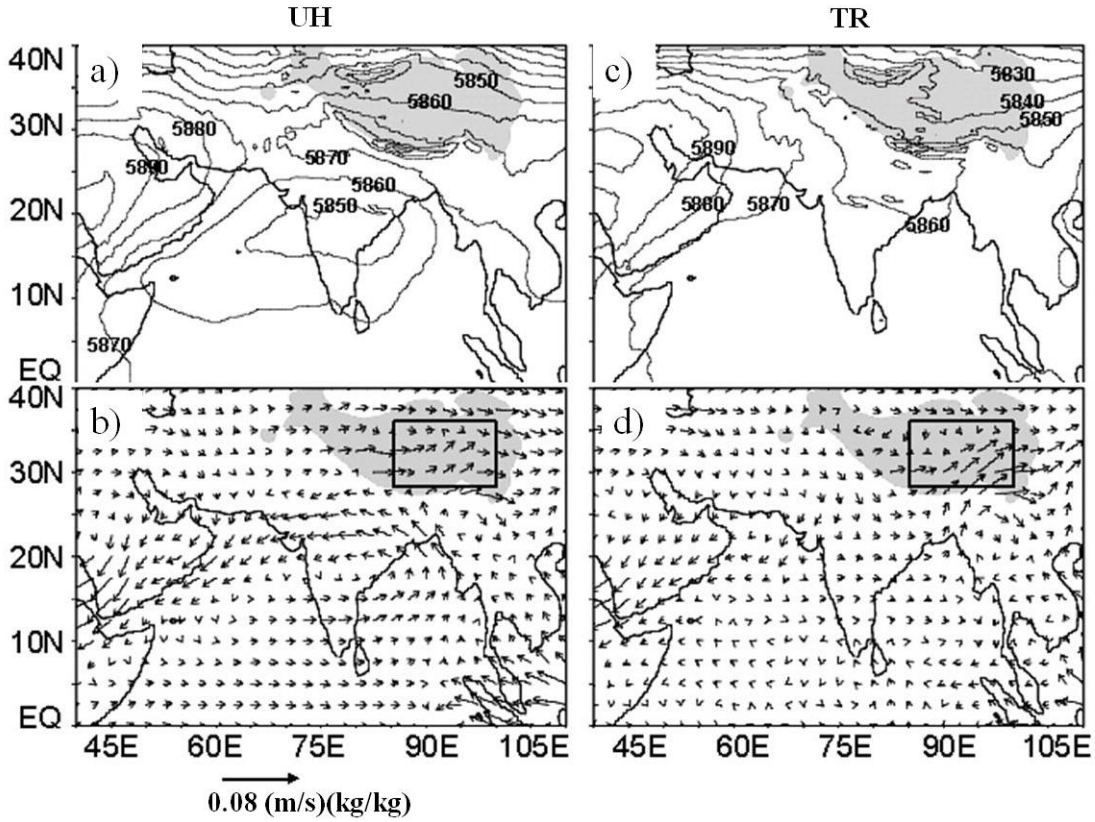

Fig. 3.3. Same as Fig. 3.2, but for 500 hPa. Areas higher than 3000 m are shaded light gray at 500 hPa. Open boxes in b) and d) correspond to Box A in Fig. 2.1.

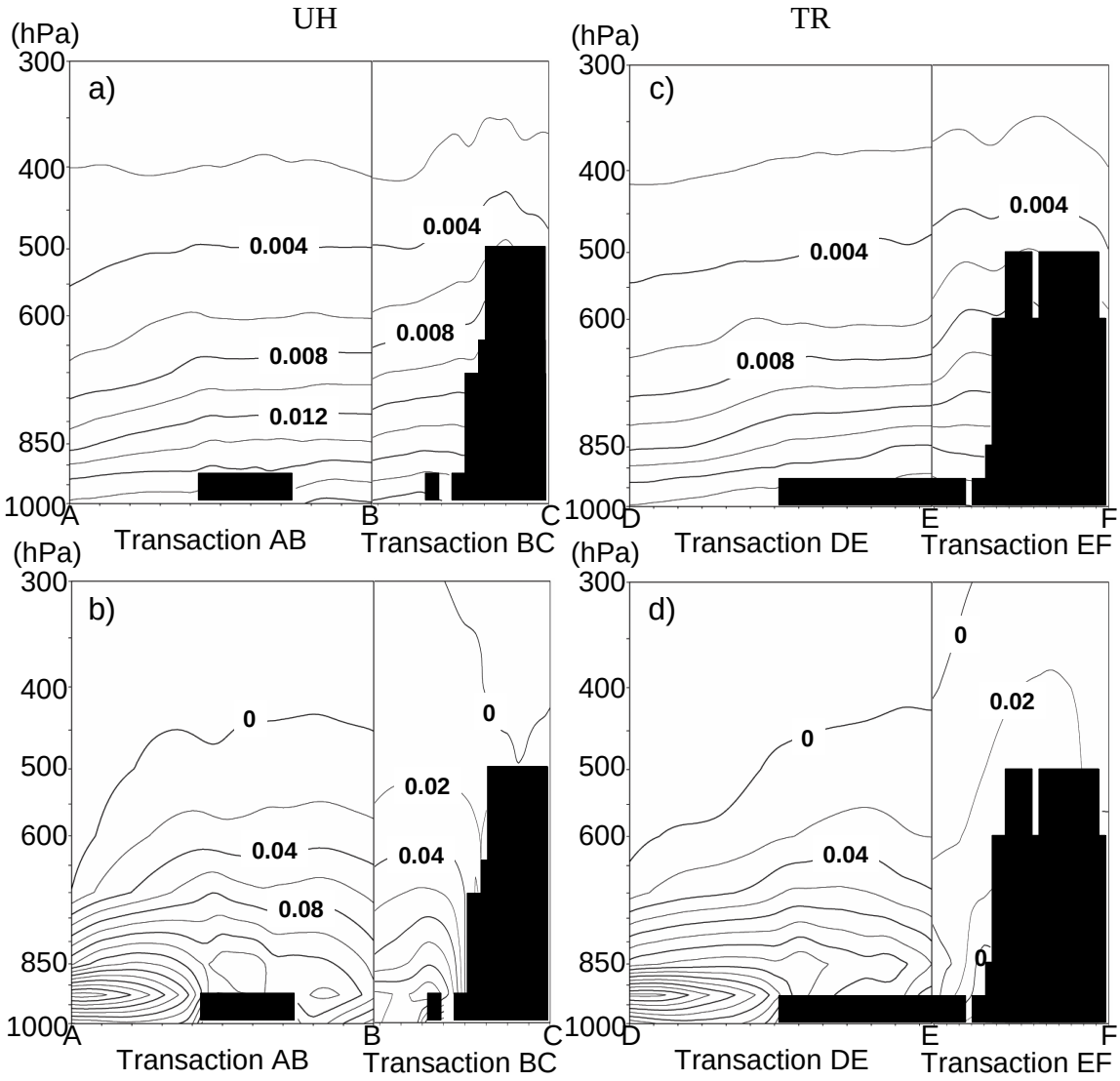

Fig. 3.4. Height cross-sections of specific humidity (upper) and WV flux (bottom) in the case of the UH type (left) and TR type (right). The cross-sections for the UH type is along the transection A-B-C in Fig. 3b, and that for the TR type is along D-E-F (right) in Fig. 3f. The contour interval of specific humidity (kg/kg) is 0.002, and that of WV flux (kg/kg × m/s) is 0.02. Topography is shaded black.

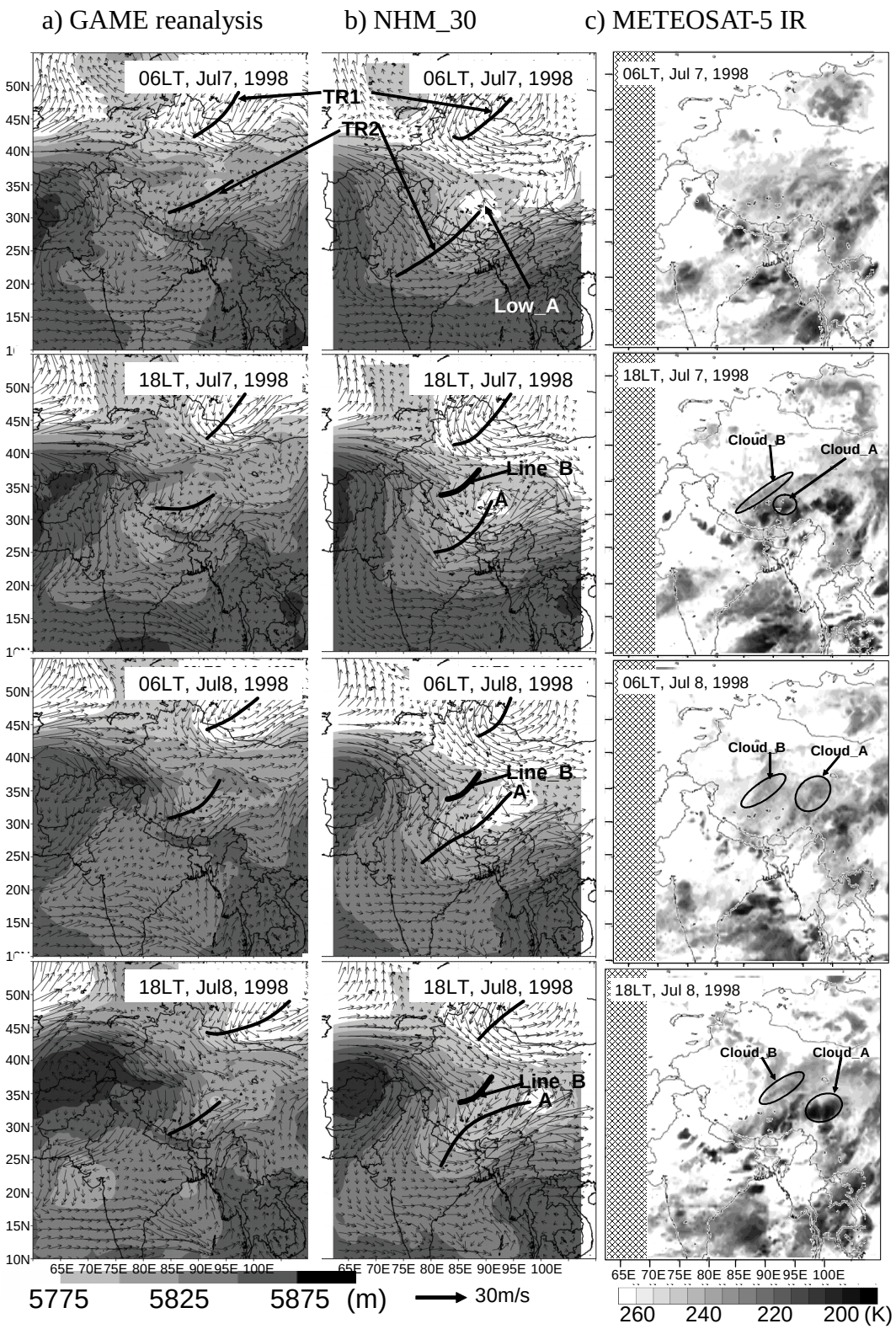

Fig. 3.5. Geopotential height and wind vector at 500 hPa for a) GAME reanalysis data, b) NHM_30, and c) METEOSAT-5 IR images at 06 and 18 LT on July 7-8. TR1and TR2 indicate two troughs. Low_A (or A) indicates a mesoscale cyclonic circulation over the TP. Line_B indicates a convergence line. Cloud_A and Cloud_B indicate convective zones accompanied by Low_A and Line_B. These marks are explained in Section 3.2.

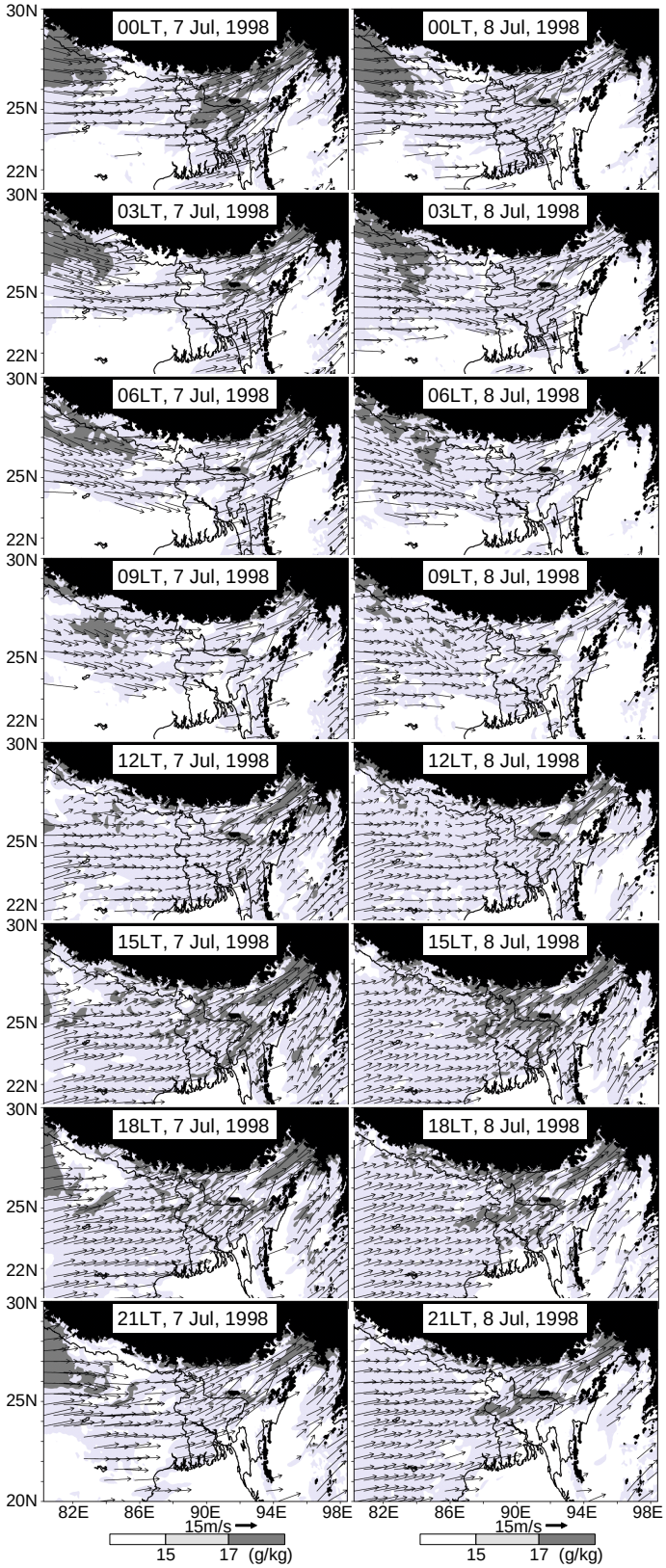

Fig. 3.6. Wind and specific humidity changes at 1500 m a.s.l. for July 7-8. Wind vectors are shown only in the shaded area. Specific humidity follows the color legends given at the bottom of the figures. Areas higher than 1500 m a.s.l. are shaded in black.

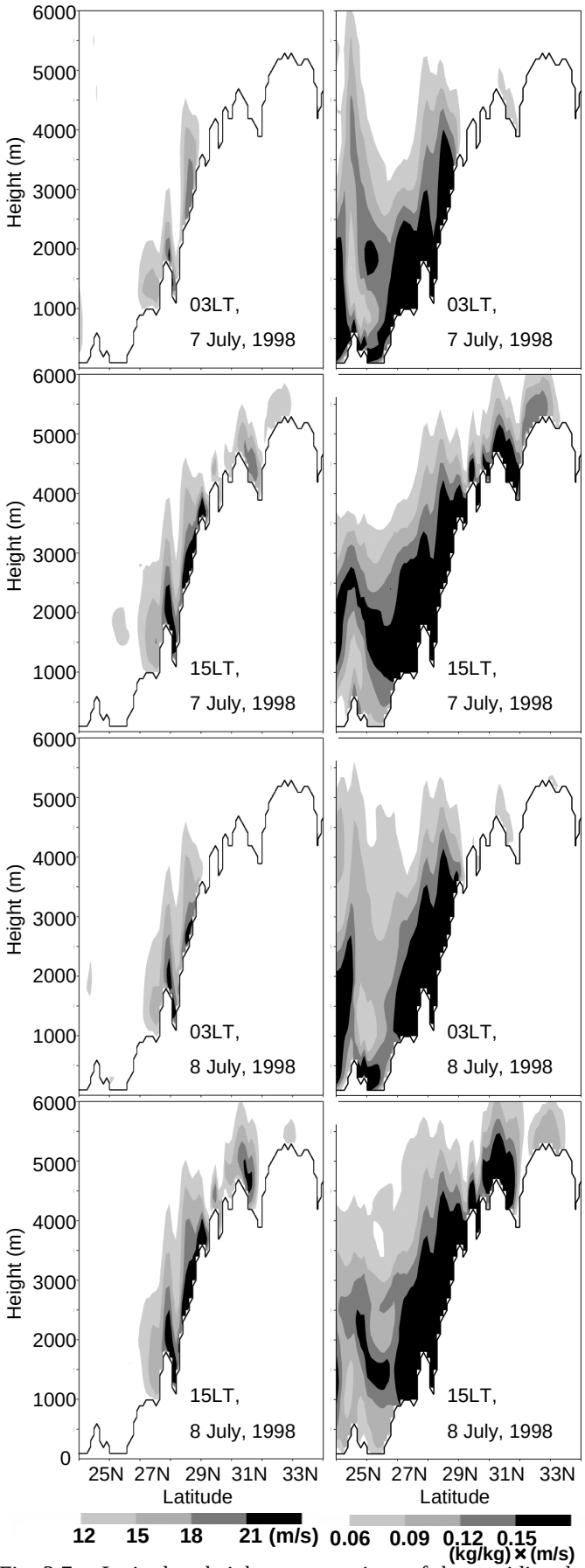

Fig. 3.7. Latitude – height cross-sections of the meridional wind speed (left) and meridional WV flux (right) along 93°E in the late night and afternoon of July 7 and 8. Thick line indicates surface elevation.

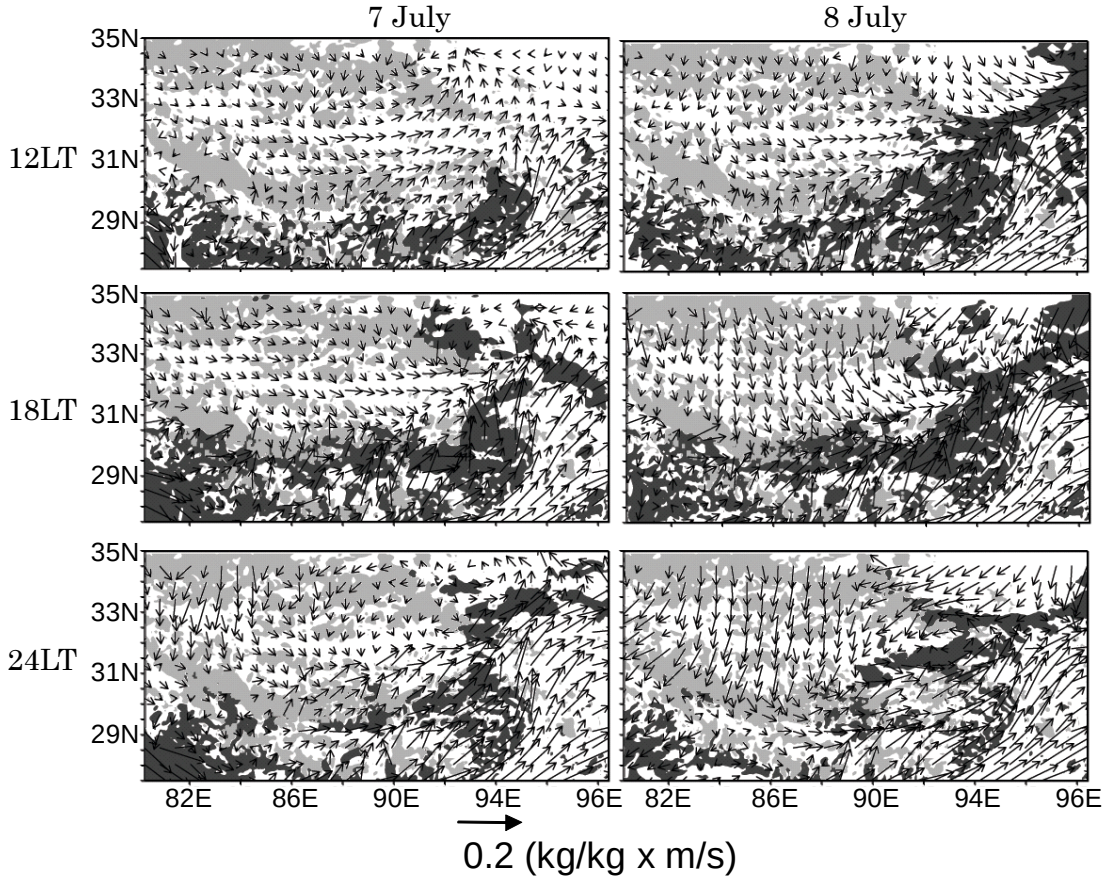

Fig. 3.8. Specific humidity (dark shade) and WV flux (vectors) at 5500 m a.s.l. simulated by NHM_6 on July 7 (left) and July 8 (right) in 1998. Dark shading corresponds to specific humidity of more than 0.008 kg/kg, and light shading shows mountain topography of more than 5000 m a.s.l.

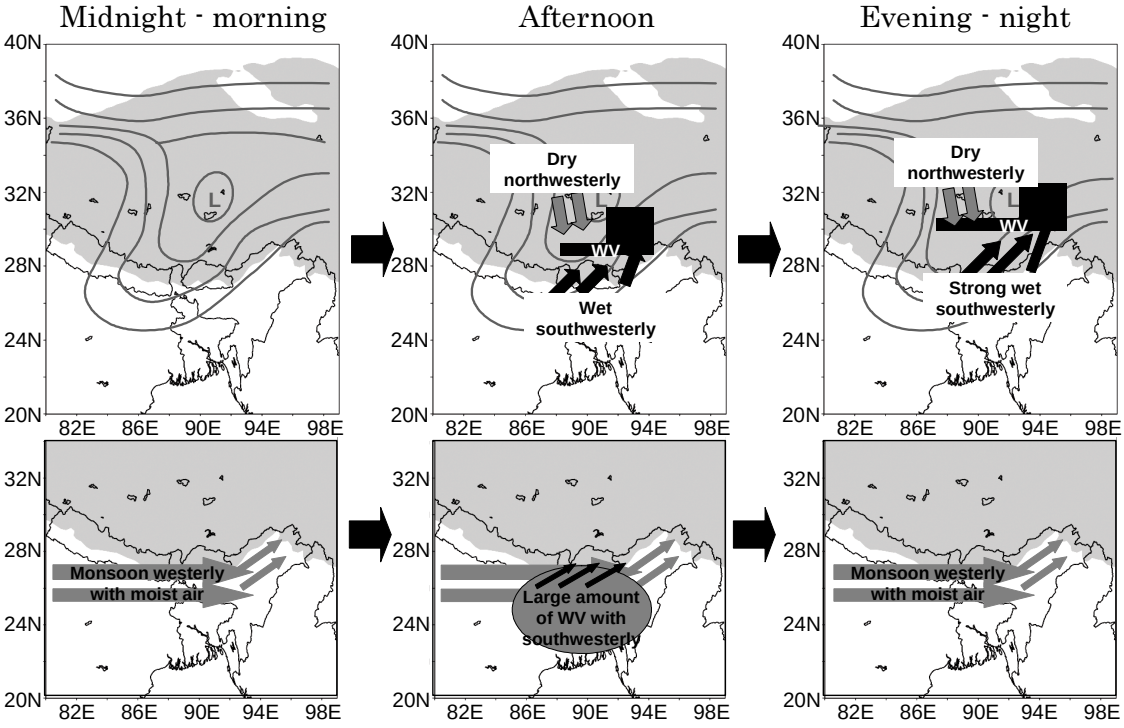

Fig. 3.9. Schematic diagrams of WV transport processes from south of the Himalayas to the TP in the TR case. Upper panels indicate the middle troposphere, and lower panels indicate the lower troposphere. Areas higher than 1500 m a.s.l. are shaded.

Chapter 4 Formation of MCSs over the eastern TP

4.1 MCS distribution and synoptic condition in cases of extensive developments

MCSs occurrence distribution was examined by method described in Section 2.3, and the mean occurrence number of MCSs extracted in the TP was 106 per year. The location of the MCSs genesis showed two maximum centers, i.e., Area A in the southern mountain area and Area B in the eastern TP, as shown in Figure 4.1a. The intensive distribution of Area A was identified by Barros et al. (2004), but that of the Area B was not shown because it was outside of their analysis area. On the other hand, the two maximum centers corresponded well with those described by Li et al. (2008). The distribution of the extinct location of the MCSs is also shown in Figure 4.1b. The MCSs in Area A disappeared at a similar location of its occurrence. However, the MCSs generated in Area B moved southeastward, and some of them vanished out of the TP. There was positive correlation between the maximal area and continuance (or migration length) of the MCSs in Area B (no figure). Therefore, the large MCSs in the eastern TP had a long lifetime and tended to propagate long distances to go outside of the TP.

Next, the occurrence time of large MCSs was examined. The top (low) 60 cases of the max size of the MCSs, described as Large (Small)_MCSs, were chosen in Area B, and the initial and max time were examined. For about 80 % of Large_MCS cases, the MCSs were generated in the afternoon (12-15 LT) and reached their maximal size during the evening and through the night (16-23 LT). The initial time of Small_MCS cases was irregular, between 12 and 23 LT,

and the MCSs reached their maximal area during the evening through early the next morning. To identify the characteristics of sub-continental scale circulations for the Large_MCS cases, geopotential heights with wind vectors were composed at the 200 and 500 hPa level on Japanese reanalysis data (JRA-25; Onogi et al., 2007). Composite fields were compared with the climatology during the mature monsoon season (from July through August in 1998-2006) in Figure 4.2. For the Large_MCS condition, the center of the Tibetan High extended over the southeastern parts of the TP in the upper troposphere (Figure 4.2b). Near-surface low pressure in the northwestern TP was more intensified than in the climatology and caused the meandering of subtropical westerlies and ridge formation on the eastern TP (Figure 4.2d). At the central plateau, the meandering westerlies converged with southwesterlies intruding from northern parts of the Bay of Bengal. This southwesterly was induced by the enhancement of cyclonic circulation with a low-pressure area over the Indian subcontinent in the mid-troposphere. According to Yamada and Uyeda (2006) and Sugimoto et al. (2008), those features of the synoptic circulation corresponded in the active phase of the Plateau and Indian monsoon, when land-surface heating was dominant without overpowering synoptic trough condition. Additionally, low-level convergence formation over the central TP was similar to that at the low-vortex occurrence timing, as shown in Zhang et al. (1988). On the other hand, the composition for the Small_MCS cases showed that the upper tropospheric Tibetan anticyclone did not expand to the east and the near-surface convergence weakened with no meandering westerlies under the decayed low-pressure condition in the western plateau (no figure). In the case of no MCS formation, the eastern TP covered the high pressure at 500 hPa because it was

located at the rear of the synoptic trough. Namely, large MCSs were generated intensively during the daytime by the dominant land-surface heating with the low-level convergence under the condition with a prevailing upper tropospheric Tibetan anticyclone.

In order to reveal the effect of the established low-level convergence under the strong land-surface heating condition on the large sized MCS formation over the eastern plateau, the diurnal evolution of the near-surface pressure and winds was examined with Tbb anomalies for the Large_MCS cases. The anomaly of the wind and geopotential height at 500 hPa was calculated by subtracting 6-hourly averaged JRA-25 data for all analysis period days from that for 60 days of Large_MCS cases. On the Meteosat5-IR data, the convective index (Ic), defined as Ic=250-Tbb if 250-Tbb is positive or Ic=0, was calculated, and the Ic anomaly was composed in the same way. Figure 4.3 shows the 6-hourly interval of composed anomaly patterns starting from 24 hours prior to the evening, when the Large-MCS development was recognized in Area B of Figure 4.1.

In the evening of one day before the MCS genesis (Figure 4.3a), a low-pressure anomaly distributed in the northern plateau with its center at around 36N/90E, corresponding to the expansion of the depression emphasized in Figure 4.2d. The convergence anomaly was recognized along the southern periphery of the low-pressure anomaly, where the active convection zone appeared (Figure 4.3f). The distribution of the active convection zone was similar to the highly frequency zone of the low vortex and hailfall occurrences analyzed by Tao and Ding [1981]. The anomaly pattern persisted until midnight (Figure 4.3b and 4.3g), and the low-pressure anomaly gradually moved eastward with weakening of convections until noon of

the next day (Figure 4.3d and 4.3i). Then, strong convection started over the eastern edge of the plateau in the evening and developed into large MCSs. The composite maps suggest that the occurrence of large-scale MCS in the eastern TP was induced by the strong convergences due to the migration of thermally induced cyclonic circulation formed one day prior to the MCS genesis. To recover the limit of reanalysis data and to understand the three-dimensional structures of the circulations within the plateau, a numerical simulation with finer spatial resolution was performed for the representative cases of the development of Large_MCSs in the following sections.

4.2 Processes of MCS genesis in WRF simulation

In the 60 days of Large_MCS occurrences in Area B, three days with significant low-pressure propagation near the surface were selected for the numerical experiment, i.e., Jul. 4 in 1998, Jul. 2 in 2000, and Aug. 26 in 2005. The detail numerical design was shown in Section 2.5. Simulation results for the case of Aug. 26, 2005 were compared with JRA-25 and Meteosat5-IR images at 500 hPa (Figure 4.4). The cloud-top temperature in the simulation was interpreted by the temperature at the highest layer with cloud water or cloud ice more than 0.1×10^{-4} kg/kg. In the noon of one day before the MCS genesis (Aug. 25), a low-pressure area was analyzed over the northwestern TP in both the reanalysis and simulation results (Figure 4.4a and 4.4b). Cyclonic circulation with a low-pressure area developed at 18 LT (Figure 4.4c and 4.4d) and moved eastward from 24 LT (Figure 4.4e and 4.4f) to 12 LT the next day (Figure 4.4i and 4.4j). However, in the WRF simulation, cyclonic circulation by the low-pressure system

strengthened the westerlies over the southwestern plateau from evening to midnight (Figure 4.4d and 4.4f). The enhanced westerlies induced convergences over the southern plateau with easterlies associating with anticyclonic circulation at the east side, and this feature was not analyzed in the JRA25 data. Scattered clouds were reproduced in the convergence area by the simulation, and a similar cloud pattern was found in the Meteosat5-IR image. Namely, the WRF could simulate realistic convergence zones to diagnose the three-dimensional circulation structures.

In the Meteosat5-IR image, MCS was generated at 14 LT on Aug. 26 and developed in the southeastern plateau during the evening (Figure 4.4k). WRF reproduced the similar pattern of MCS genesis over the area with convergences between the northerly in the rear of the cyclonic circulation and the southwesterly (Figure 4.4l). In the case of Jul. 4 in 1998, the simulated MCS located more to the north than in the satellite images because northerly intrusion with the migrated cyclonic circulation was limited to 33N (Figure 4.5a). In the case of Jul. 2 in 2000, weakening of southwesterlies prevented the westward expansion of the MCS in the WRF (Figure 4.5b). However, the systematic development of clouds and MCS, such as the establishment of low pressure one day before and traveling of the cyclonic circulation to form a low-level convergence to trigger the MCS genesis, was quite similar to that in the first case. Accordingly, I concluded that the diurnal development and migration of thermally induced cyclonic circulation from the western part played a fundamental role in the formation of large-scale MCSs in the east.

To understand the systematic mechanisms of MCS generation with the migration of

cyclones, the three-dimensional output of WRF simulation in Aug. 25-26, 2005 was intensively diagnosed. One day before the MCS genesis, 15 LT on Aug. 25, the surface sensible heat flux was large in the western plateau due to drier land-surface conditions (Figure 4.6a). This feature agreed with observational results by Xu and Haginoya (2001) and Xu et al. (2005), who mentioned that the sensible heat flux was dominant in the western TP during the mature monsoon season. Strong sensible heating warmed the near-surface atmosphere that advected northeastward and formed the 800-1000 km-scale low-pressure area, as shown in 500 hPa (Figure 4.6b). At this moment, the low-pressure system was shallow and identified below 400 hPa (Figure 4.6c). During the daytime, cloud formation was neither simulated in the low-pressure system nor observed in the Meteosat5-IR images, indicating that the system was not caused by latent heat release with condensation. Consequently, the low pressure formed over the northwestern TP was recognized as a “thermal low” induced by strong daytime sensible heating under dry land-surface conditions. In the thermal low, southwesterlies converged at around 85-91E along the 36N with northerlies induced by the intensification of upslope winds over the northern peripheries of the plateau. Cyclonic circulation occurred in the eastern end of this convergence zone at 18 LT (marked L in Figure 4.4d) and remained after sunset. This process would correspond to the formation of a low vortex by Zhang et al. (1988), who described that a cyclonic vortex was generated by strong land-surface heating over the western plateau and wind shear between northeasterlies and southwesterlies.

Next, I examined the processes of the eastward movement of the low vortex. Figure 4.7a is a time sequence of positive vorticity at 500 hPa with averaged zonal wind speed in

400-450 hPa from Aug. 24 to 27 along the 30-37 N zone in which the moving low vortex was analyzed. Increase of daytime wind speed and stronger positive vorticity in the late evening were found in the western areas, around 81-93 E, indicating that thermally induced low pressure system developed most of the days with the development of a mixing layer. Through Aug. 25 to 26, evident eastward propagation of the positive vorticity with a phase speed of about 0.67 degrees per hour started from the central plateau, which was consistent with the eastward movement of stronger westerlies areas, as marked by a white arrow. The layer with positive vorticity larger than $1.0x10^{-4}$ (s^{-1}) reached approximately 370 hPa, where westerlies of about 20 m/s were dominant after 00 UTC on Aug. 26, and the phase speed was mainly controlled by wind speed near the top level of positive vorticity. Upper tropospheric anticyclonic circulation prevailed with the center at 93E/28N, and a mid-latitude trough was approaching from west of the TP in the early morning of Aug. 25 (Figure 4.8a). The composition of the synoptic chart of Large_MCS cases (Figure 4.2b) also indicated the existence of a synoptic trough in the west of the Tibetan High in the upper troposphere. Zhang et al. (1988) pointed out that a low vortex migrates eastward when it occurs just under the northern part of the Tibetan High, and our three simulated cases agreed with their results. In Figure 4.8, the southern part of the trough gradually tilted eastward, and a stronger geostrophic wind area ahead of the trough also moved eastward over the northern TP.

In two other cases, on Jul. 3-4, 1998 and Jul. 1-2, 2000, there were also areas of eastward propagation of positive vorticity starting from the western TP two or three days before the MCS genesis and passing over the central TP a day before it (Figure 4.7b and 4.7c) with

different phase speeds, such as 0.17 and 0.42 degrees per hour respectively. Both of the cases showed similar circulation patterns in the upper troposphere, as shown in Figure 4.8, except that surface westerlies were weaker in 1998 and produced a slower propagation speed. According to this evidence, I assumed that the near-surface migration of the low vortex was controlled by the enhancement of upper tropospheric westerlies under conditions of a prevailing Tibetan High and the approach of the synoptic trough from the west.

In the afternoon on Aug. 26, the migrated low vortex was intensified with daytime surface heating over the eastern plateau, and it induced low-level convergences between northerlies and southerlies where the MCS was generated at 15 LT (Figure 4.9a). In the vertical cross cutting along the convergence (Figure 4.9b), the increase of the equivalent potential temperature in the lower troposphere due to moistening by the largely latent heat flux over the wetter land-surface condition (Figure 4.9c) strengthened convective instability in the south of 35N, and the instability contributed to the development of large MCSs in the evening. In two other cases, similar structure of low-level convergence and instability was recognized, such that southwesterly in the eastern TP converged near surface with northerly/northwesterly in rear of the migrated low-vortex, and the strong convective instability formed by surface latent heat flux (no figure). Consequently, the low-level convergence due to migration of low vortex and surface latent heat flux forming the convective instability were suggested as two key factors for the generation of MCS in the southeastern TP areas by the numerical simulation.

4.3 Impact of land-surface fluxes on the formation of MCSs

The longitudinal gradient of the surface wetness over the plateau provides a fundamental condition for the development of thermal lows in the west and convective instability in the east. To investigate the effects of the two factors for MCS generation, two sensitive experiments were carried out by a WRF numerical simulation for the previous three MCS cases; one experiment removed the sensible heat flux larger than 250 W/m^2 at land surface over the areas exceeding 3000 m until the day before the MCS genesis (noHFX run), and the other one removed the latent heat flux larger than 125 W/m^2 on the day of the MCS genesis (noQFX run). Accordingly, the sensible (latent) heat flux dominated in the western (eastern) plateau was cut off, as shown in Figure 4.10b and 4.10d.

The evolution of circulations near the plateau surface and the MCS genesis are compared for Aug. 25-26, 2005 in Figure 4.12. In the case of the NoHFX run, the low pressure area in the western plateau calculated in the Ctl run (Figure 4.11a) was abruptly weakened at 18 LT before one day of the MCS formation (Figure 4.11d), which assured that the system was the thermal low, and the eastward propagation of the low vortex was not simulated (Figure 4.11e). Therefore, convergence in the eastern plateau was weakened in the Aug. 26 afternoon, and convections did not develop into MCS (Figure 4.11f). In the case of the noQFX run, circulations before the morning of Aug. 26 was same as those in the Ctl run (Figure 4.11g and 4.11h). However, MCS was not generated in the south of the low-pressure area (Figure 4.11i). The profiles of an equivalent potential temperature at 15 LT, averaged in the domain of 30-35N/98-102E, were compared between the Ctl and NoQFX runs (Figure 4.11). Below 480

hPa, strong convective instability in the Ctl run was dissolved in the NoQFX run, and abrupt development of MCS in the Aug. 26 evening was prevented. The same sensitivity experiments were performed for the cases on Jul. 3-4, 1998 and Aug. 25-26, 2005. For the NoHFX run, weakening of the low-level convergence did not induce the MCS formation of the case of Jul. 1-2, 2000, as in the case of Aug. 25-26, 2005. On the other hand, clouds were generated in the subtropical westerlies in the northeastern part of the plateau in the morning and organized in the afternoon for the case of Jul. 3-4, 1998. However, this developed cloud system was smaller than that of the Ctl run. For the noQFX run, the MCS was also not generated in either case due to the decrease of the convective instability corresponding with the removal of the latent heat flux. The sensitivity experiments assured that changing of the longitudinal gradient of soil moisture in the plateau deformed the thermally induced low-pressure system in the west or low-level potential instability in the east, and, as a result, the MCS genesis in the eastern plateau was suppressed.

4.4 Summary

Diurnal evolution of MCS genesis in the eastern TP during the monsoon season was analyzed using reanalysis data and satellite images, and three-dimensional formation processes were diagnosed by numerical experiments focusing on the contrasts of plateau-scale surface-heating components. The content in this chapter are submitted by Sugimoto and Ueno (2009), and major results are summarized as follows:

1) MCS genesis, identified in the 9-year Meteosat5-IR images, was concentrated in the eastern

and southern TP, as shown in previous studies. Composite analysis of the reanalysis data and IR images for the cases of large MCSs in the eastern TP were characterized by eastward magnification of an upper tropospheric anticyclone with intensification of near-surface low pressure in the western plateau and enhancement of the low-level longitudinal convergence line in the central TP. Diurnal changes of near-surface circulations were composed by eastward propagation of a cyclonic low-pressure system and associated development of low-level convergences that agreed with convective areas detected on the satellite images.

2) In the numerical simulation, before the day of the MCS genesis, thermally induced low pressure occurred over the western TP, corresponding with a large sensible heat flux under the dry land-surface condition in the daytime. The low vortex moved eastward with the intensification of the westerlies, which were induced by stronger geostrophic winds over the northern plateau under the Tibetan High development centered over southern TP and the approach of the synoptic trough. In the eastern plateau, low-level convergence between the northerlies and southwesterlies was caused in the rear of the migrated low vortex, and an MCS was formed, in correspondence with large convective instability over wet surface conditions.

3) A sensitive experiment by cutting off the sensible heat flux over the western TP simulated the weakening of a low vortex in the west, and no MCS in the east was generated on the following day. In addition, no MCS developed in the experiment involving the cutting off of latent heat flux over the eastern TP due to the weakening of low-level convective instability.

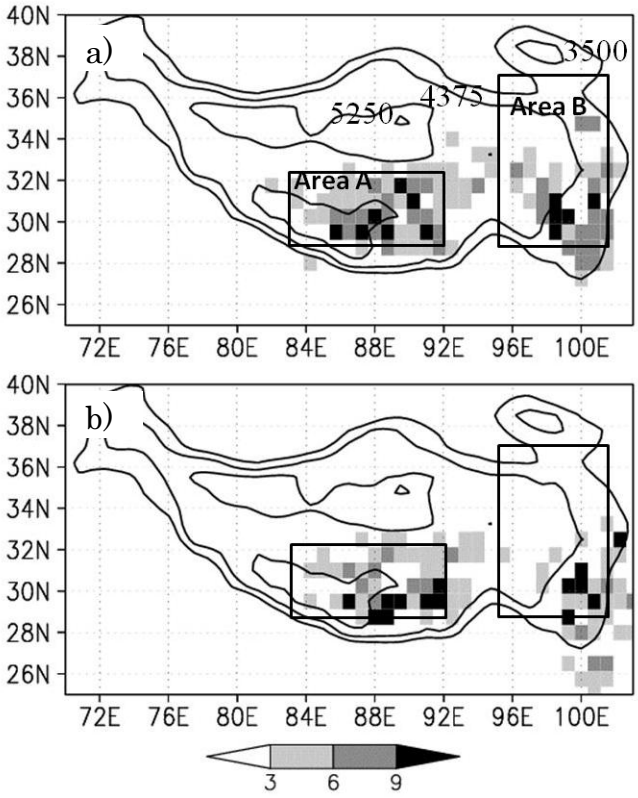

Figure 4.1. a) Frequency distribution of MCS occurrence counted at every 0.75 degrees of grid spacing during summer from 1998 to 2006. Elevations are contoured with an 875 m interval. b) Same as a), except for the frequency distribution of MCS decay.

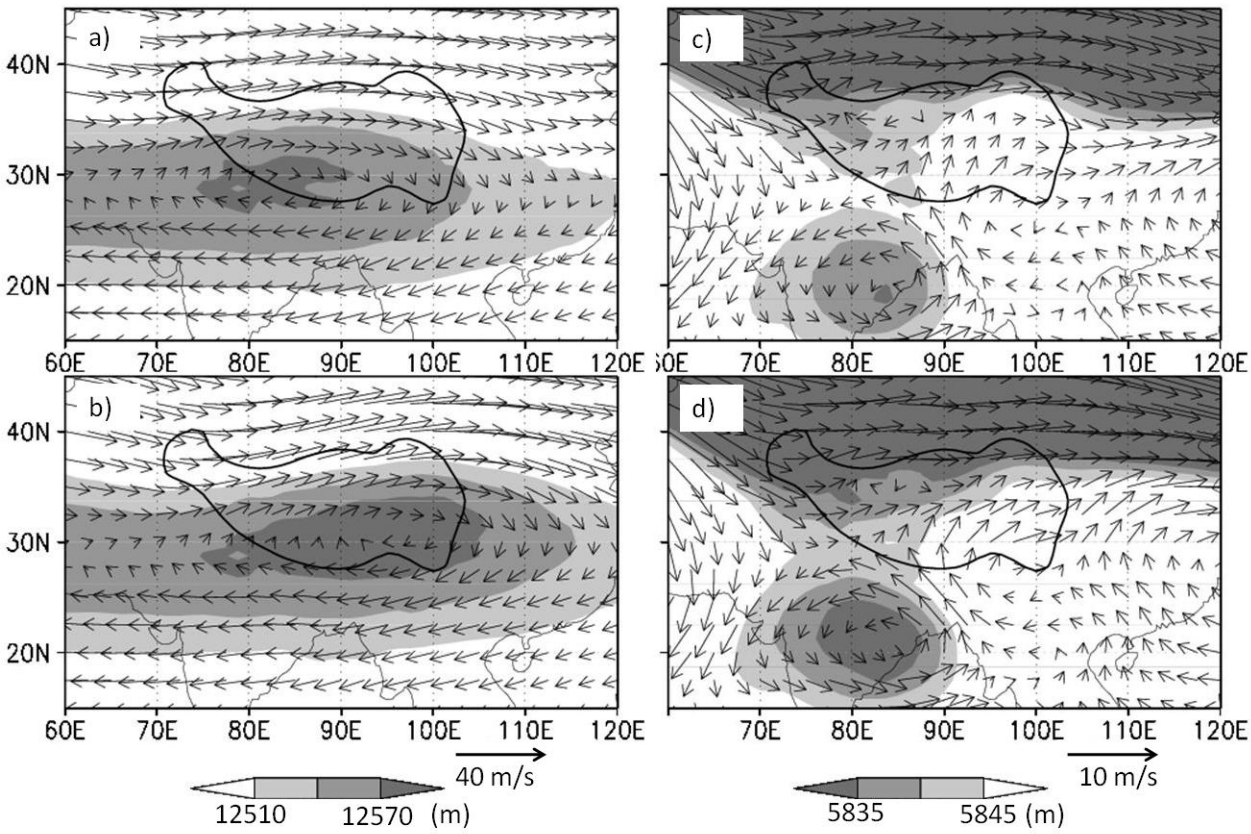

Figure 4.2. Wind and geopotential height averaged at a) 200 hPa and c) 500 hPa during the analysis period. b) and d) are the same as a) an c), except that they are averaged in the days with Large_MCS.

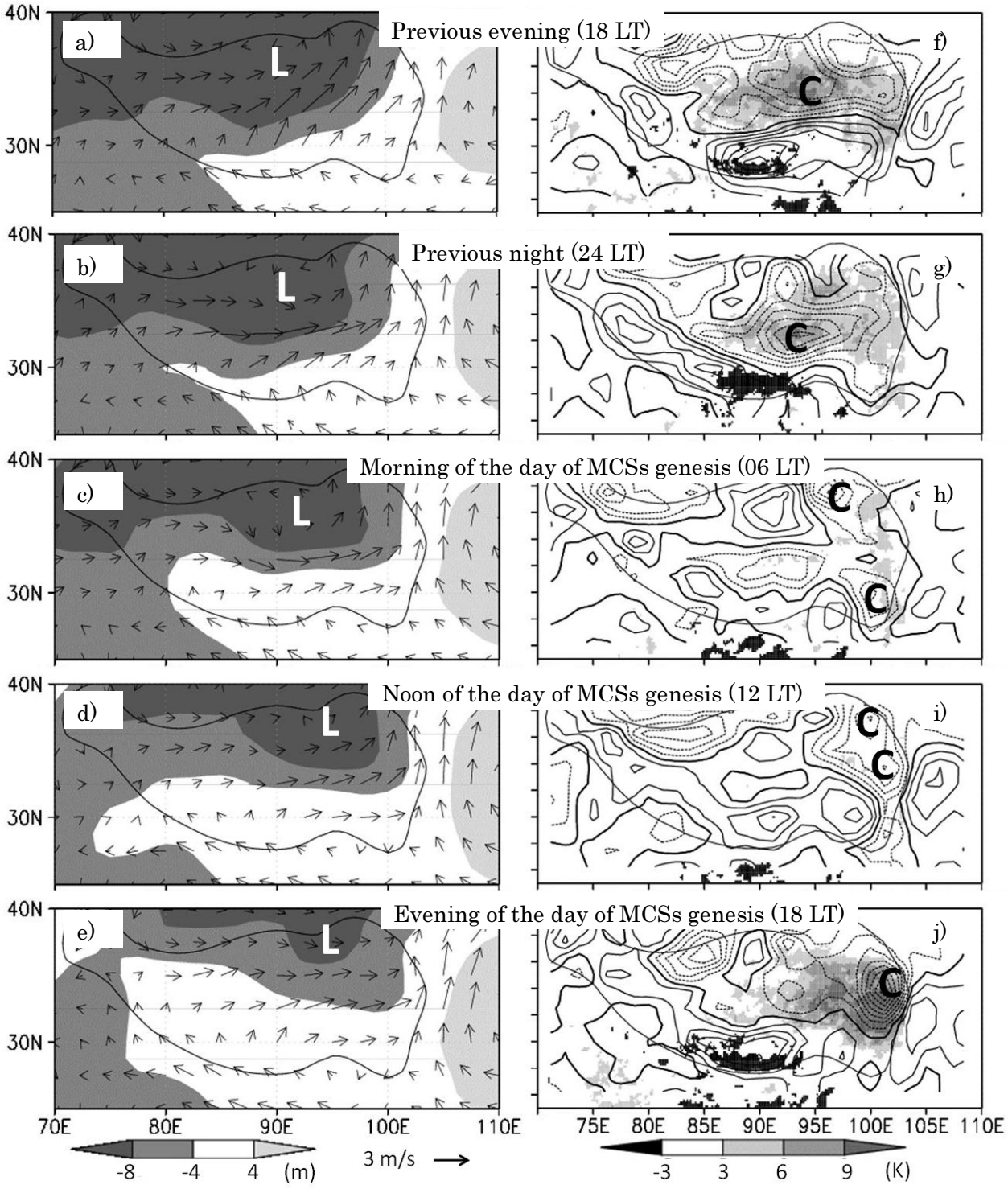

Figure 4.3. Six-hourly anomaly distribution of a)-e) wind and geopotential height at 500 hPa, f)-j) divergence at 500 hPa and Ic. The anomaly indicates differences from the composition of Large_MCS cases to the climatorogy. The solid line in a)-e) shows the topography at 3000 m. The contour interval in b) is 0.1×10^{-5} (s^{-1}), the solid/dot line corresponds to positive/negative value, and the thick solid contour corresponds to 0 (s^{-1}). L (C) indicates the center of the low pressure (convergence) anomaly.

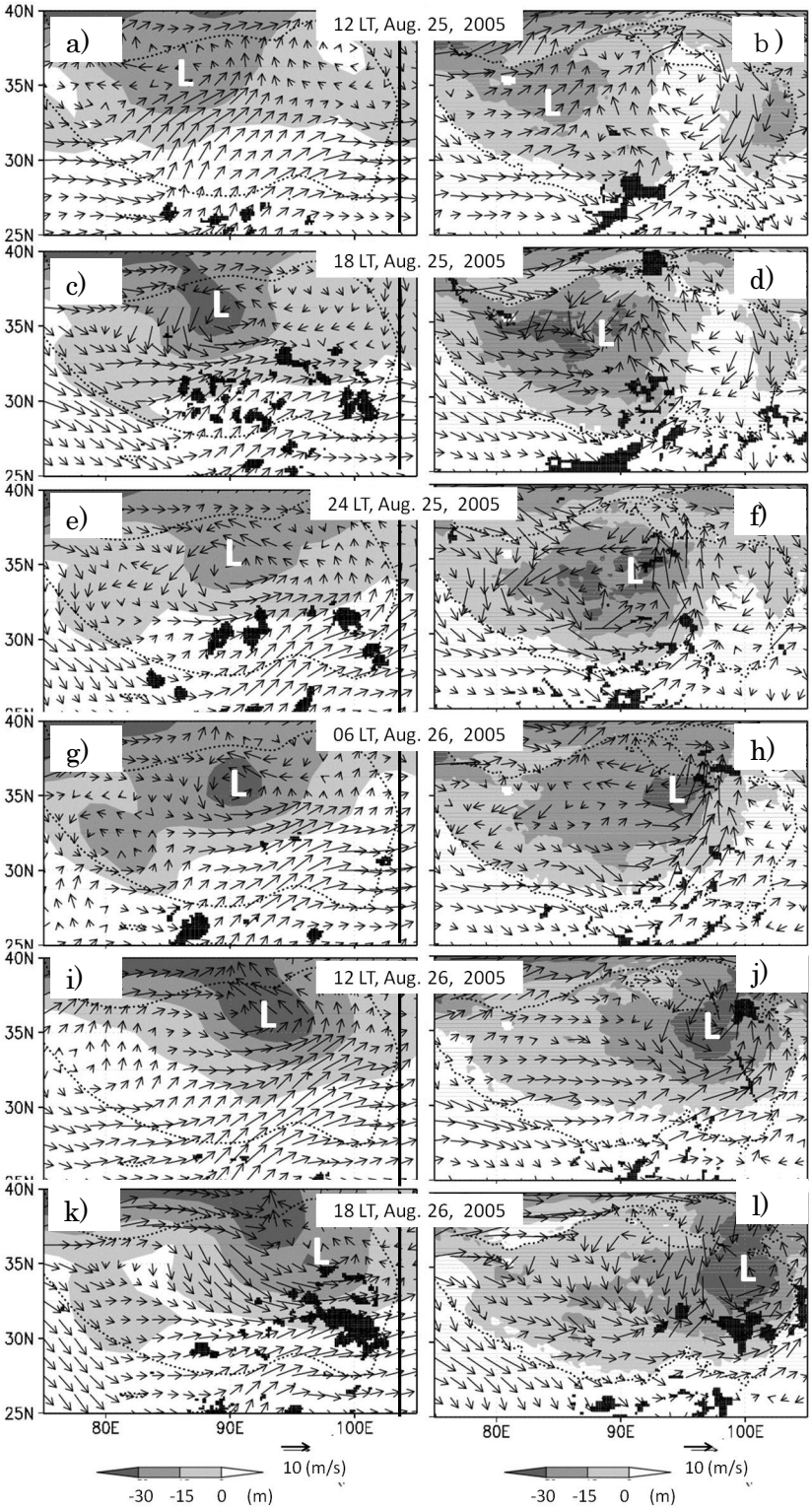

Figure 4.4. Wind vector and anomalous geopotential height from the domain-averaged (shaded), for the JRA-25 (left side) and WRF simulation (right side). Six-hourly distributions from 12 LT (06 UTC) on Aug. 25 to 18 LT (12 UTC) on Aug. 26, 2005 are shown. The black shadow indicates the Tbb of METEOSAT5 or the simulated cloud top temperature at 219 K. A dotted contour is the TP defined by the 3000 m level. L is the center of the cyclonic circulation. A black line in the figures on the left marks the eastern limit of the Meteosat5-IR images used in this study.

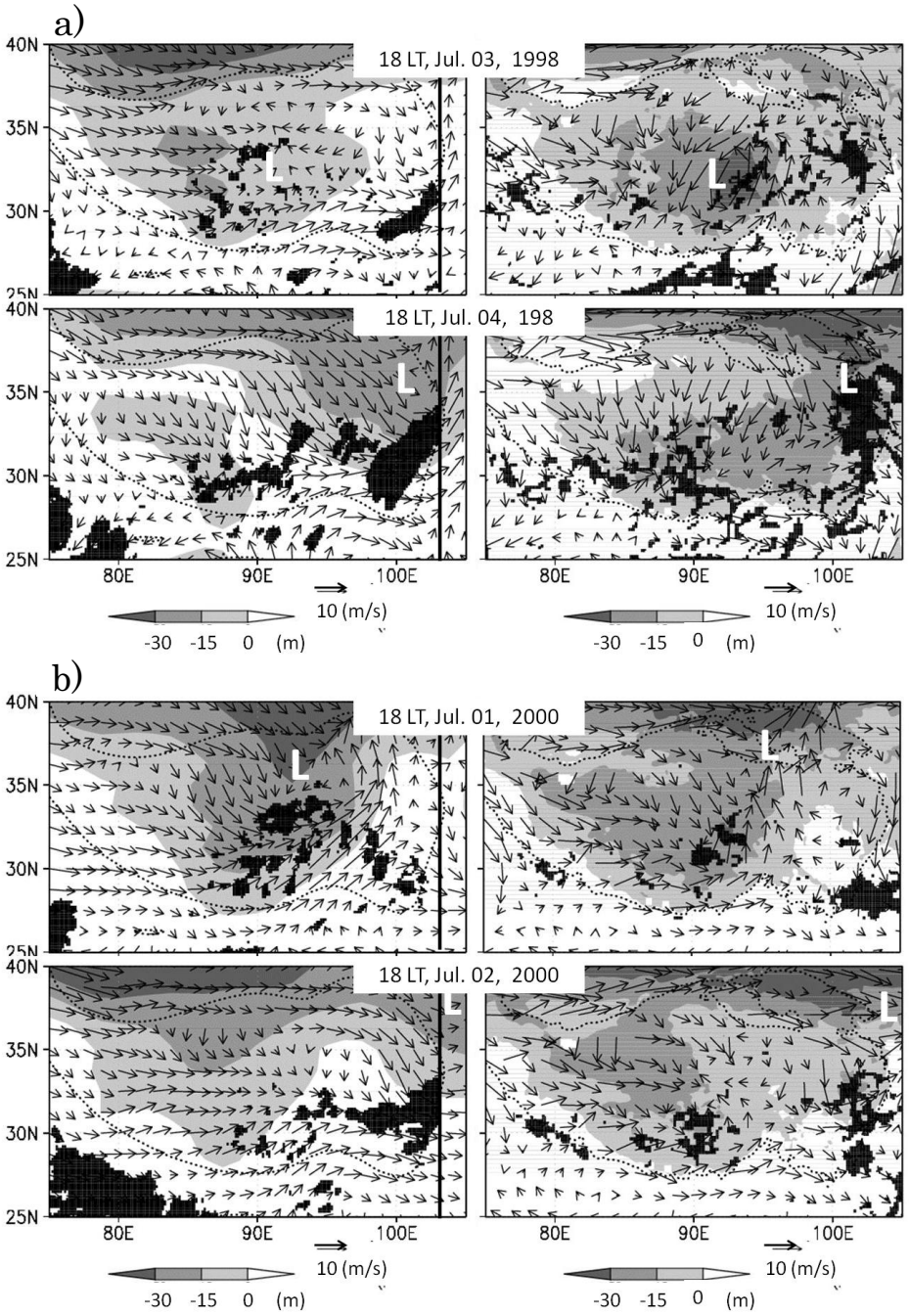

Figure 4.5. Same as Figure 4.4, but a) at 18 LT on Jul. 3 and 4, 1998 or b) at 18 LT on Jul. 1 and 2, 2000.

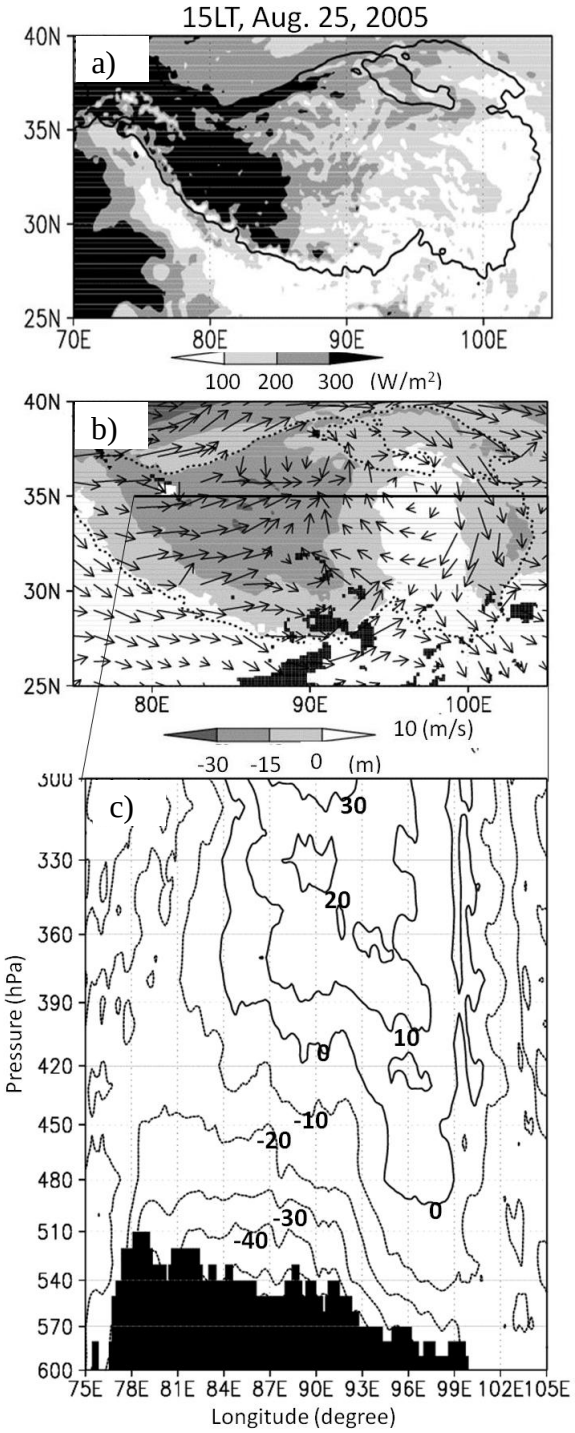

Figure 4.6. a) Distribution of the sensible heat flux, b) The geopotential height, wind, and cloud distribution are the same as in Fig. 4.4, and c) Height-longitude cross section of anomalous geopotential height (m) is domain-averaged at 15 LT on Aug. 25, 2005. A solid contour in a) shows the topography with 3000 m. The topography in c) is masked out with black.

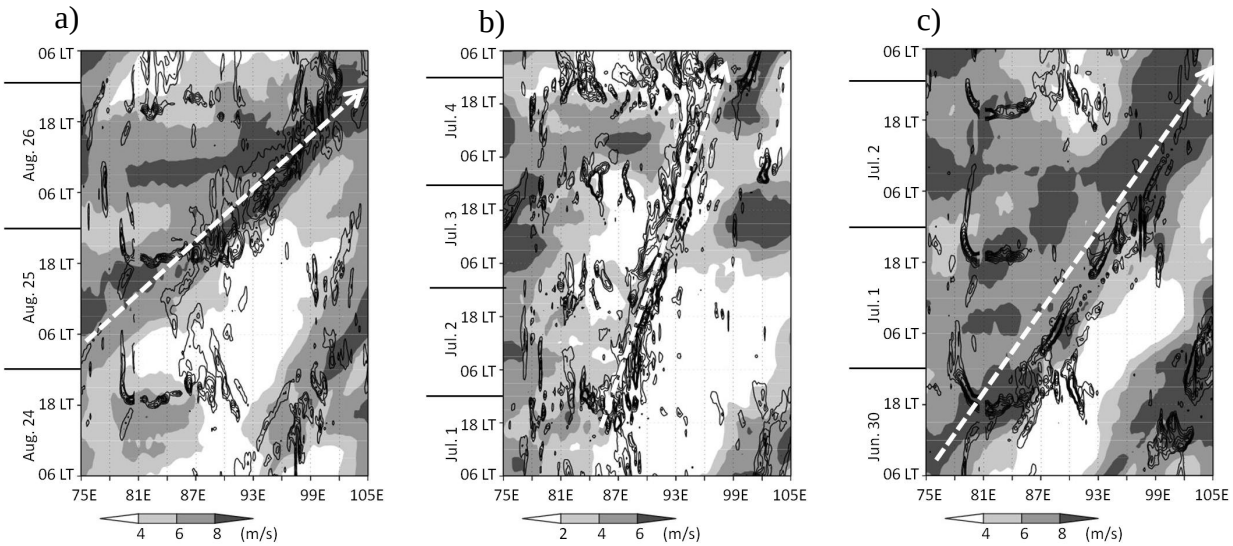

Figure 4.7. a) Time sequence of vorticity along 35 N at 500 hPa (contour) and averaged zonal wind (shaded areas) from 30N to 37N between 450 and 400 hPa from 06 LT on Aug. 24 to 06 LT on Aug. 27, 2005. The propagation of the strong westerly area is marked by a white dashed arrow. b) Same as a), but for vorticity along 32 N and averaged zonal wind between 32N and 37N from 00 LT on Jul. 1 to 06 LT on Jul. 5, 1998. c) Same as a), but from 06 LT on Jun. 30 to 06 LT on Jul. 3, 2001.

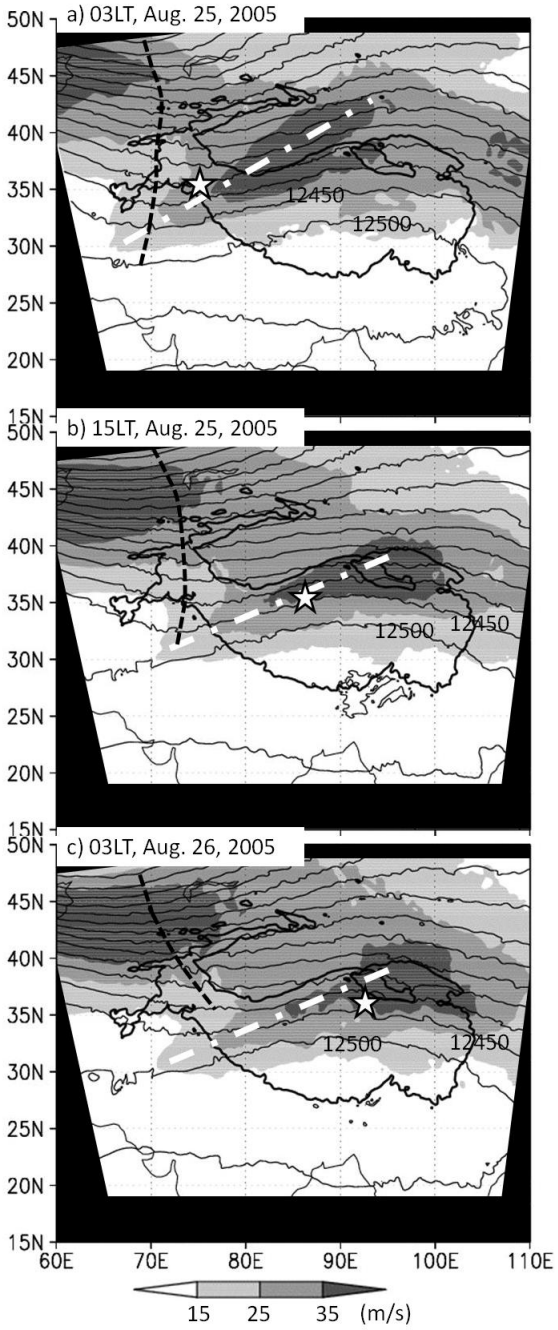

Figure 4.8. Geopotential height (m: contour with 50 m interval) and zonal wind (m/s: shaded) distribution at 200 hPa at 03, 15 LT on Aug. 25 and 03 LT on Aug. 26, 2005. The thick contour is the topography with 3000 m, and the thick dashed line is the axis of the synoptic trough. The white chain line is the enhanced zonal wind zone. The star indicates the location of the low vortex at 500 hPa. Out of simulation domain was blacked out.

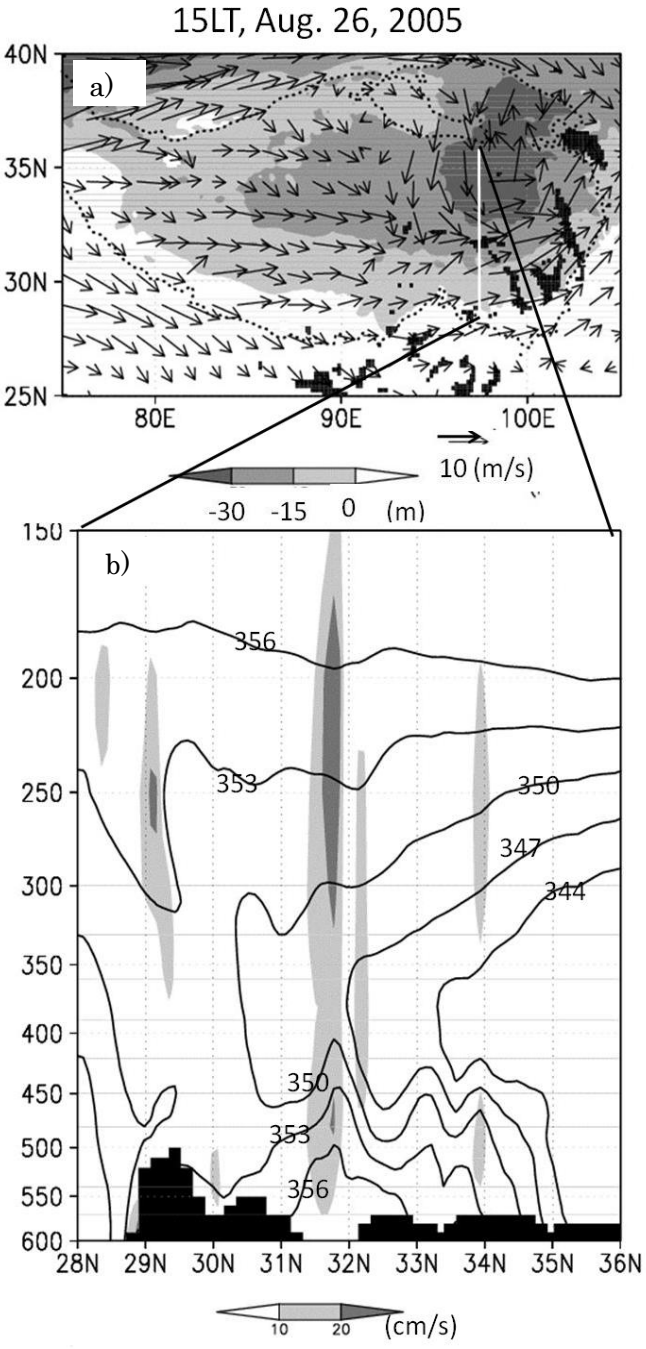

Figure 4.9. a) Same as Figure 4.4, but for 15 LT on Aug. 26, 2005. b) Height-longitude cross section of the vertical velocity (cm/s; shaded) and equivalent potential temperature (K; contour) at 15 LT on Aug. 26, 2005, along the white line in a).

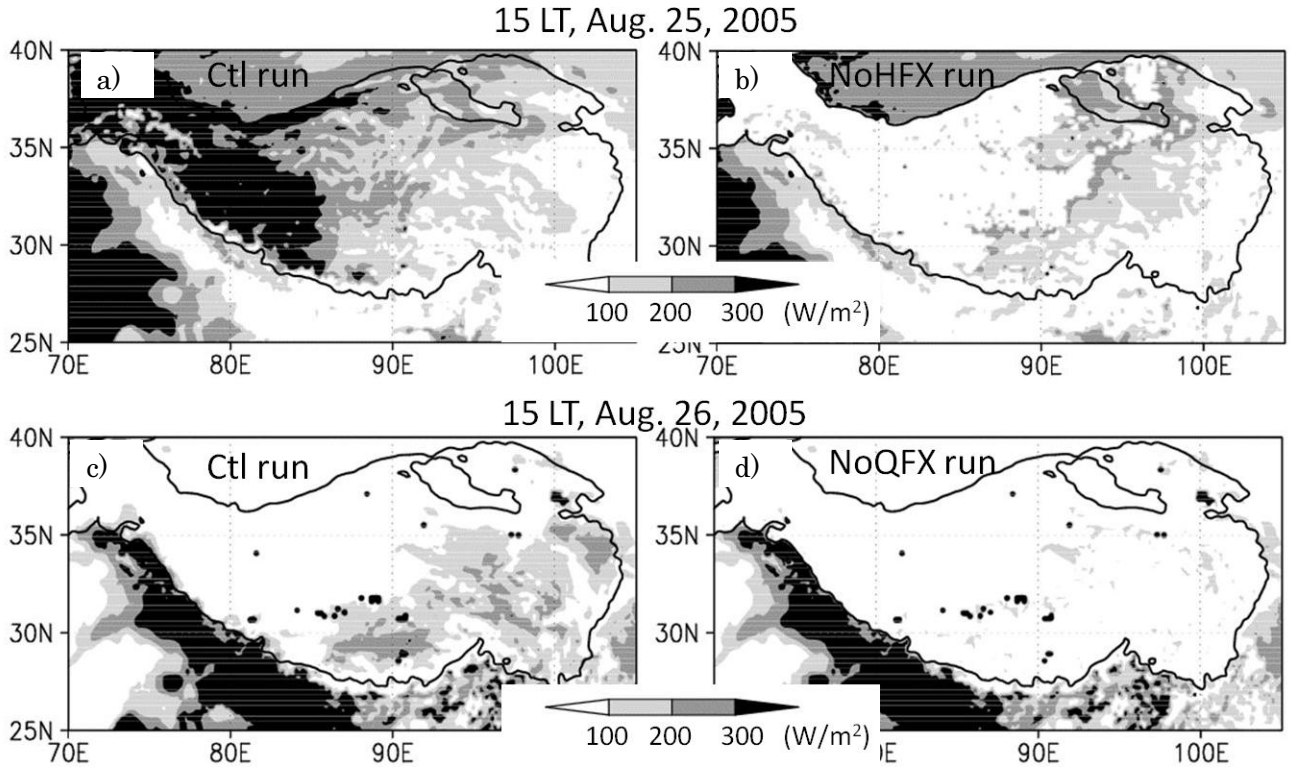

Figure 4.10. Distribution of the surface sensible heat flux for a) the Ctl run and b) the NoHFX run at 15 LT on Aug. 25, 2005. The same but for the latent heat flux for c) the Ctl run and d) the NoQFX run.

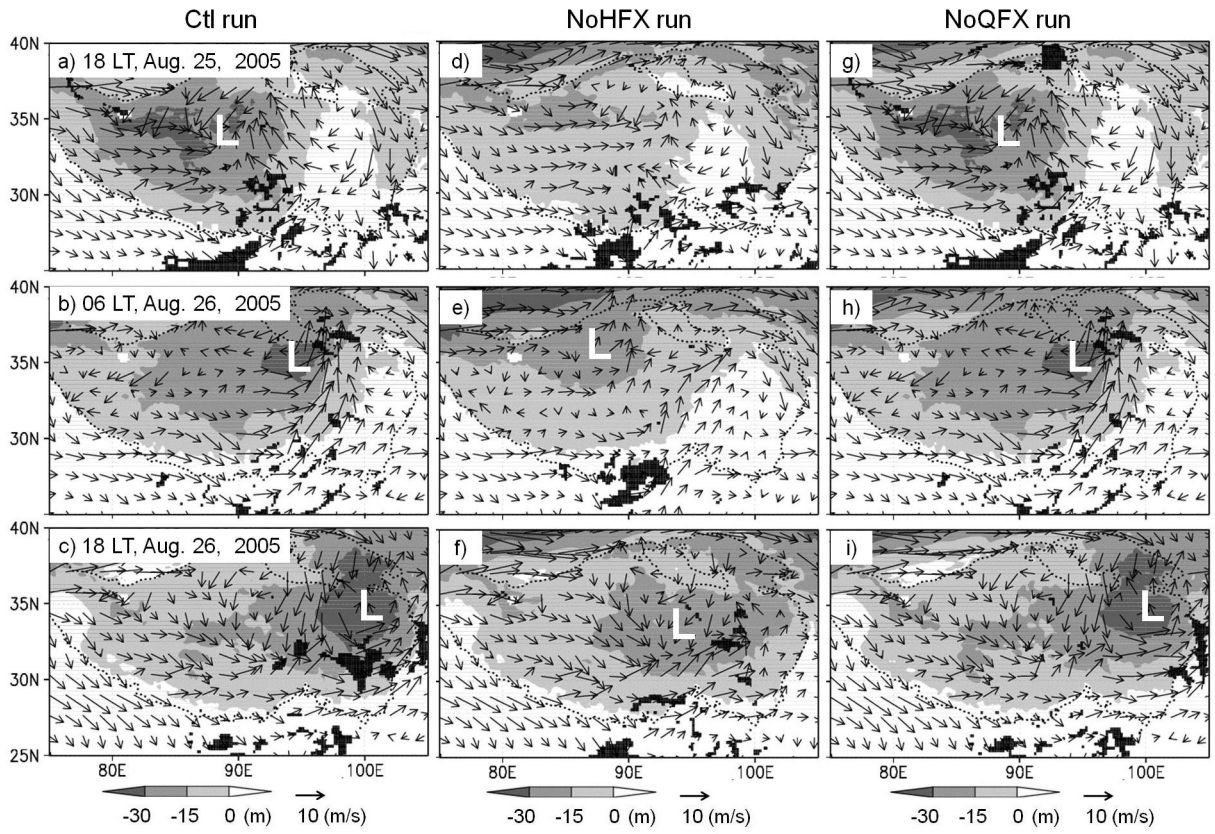

Figure 4.11. Same as Figure 4.4 but simulated in the Ctl run (left), the NoHFX run (center), and the noQFX run (right).

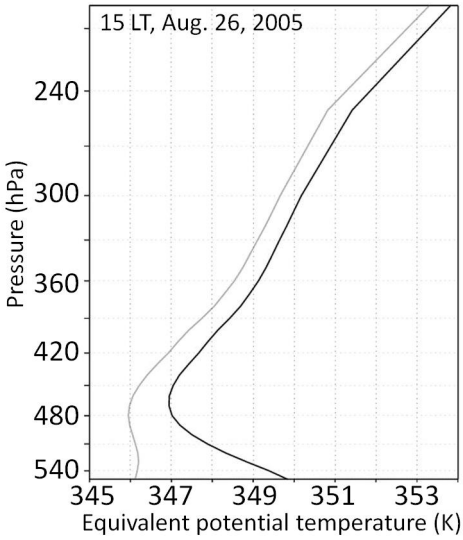

Figure 4.12. Vertical profile of the equivalent potential temperature averaged in 30-35N, 98-102E at 15 LT on Aug. 26, 2005. A black (gray) solid line indicates simulated results in the Ctl (NoQFX) run.

Chapter 5 Conclusions and Discussion

Over the Tibetan Plateau (TP), active cloud convections are formed during the summer monsoon season. We investigated transportation of water vapor (WV) into the TP and formation of mesoscale convective systems. First, I conclude finding of transport process of WV during mature monsoon season in 1998. According to WV budget analysis, significant intrusion of WV from south of the TP contributed to an increase of atmospheric moisture over the plateau in the case of a passing synoptic trough (Trough; TR type), comparing with that for the case of prevailing Tibetan High (Upper High; UH type). In the cases of UH type, monsoon westerlies passed over southern India, and its route changed towards the north with cyclonic rotation over the northern BoB in the lower troposphere. Formation of cyclonic circulation with low pressure area accompanying the active Indian monsoon phase caused transportation of WV to west and prevented the WV intrusion from south of the plateau into the middle troposphere. On the other hand, monsoon westerlies shifted to the north at 850 hPa, and moist air mass was transported directly to the southern foot of Himalayas in the case of TR type, corresponding to the break phase of the Indian monsoon. Disappearance of the low pressure area over the Indian subcontinent in the mid-troposphere allowed intrusion of WV into the TP. Diurnal variation of WV transport process into the plateau was diagnosed by numerical experiment. During early morning through afternoon, moist air mass transported by the monsoon westerlies to the southern foot of the Himalayas was lifted up to middle troposphere by development of the mixing layer and daytime enhancement of upslope wind in the southern

slope of the Himalayas. WV intrusion with southwesterlies into the TP was dominant in front of the synoptic trough from afternoon to night, and it was limited in the southeastern part of the plateau because of prevailing northwesterlies in the rear of the trough. The TR type may strongly contribute to contrasts of the ground-surface condition, such as soil moisture and vegetation, between the northwestern and southeastern TP, via a precipitation process.

Second, formation processes of the MCS are studied. Location of occurrence of MCSs was examined during the mature monsoon season from 1998 to 2006 using satellite infrared (IR) images, and it was concentrated in two areas, i.e. the southern and eastern TP. Large size MCSs with long lifetime were formed during afternoon through evening, when there was development of the Tibetan High in the upper troposphere and strong land-surface heating. The anomaly of wind and geopotential height at 500 hPa was calculated by subtracting the composite of 6-hourly reanalysis data for all analysis period days from that for Large sized MCS cases. The low pressure anomaly was identified over the northern TP before a day of the MCSs genesis and propagated eastward. At the same time, a convergence anomaly was formed at the southern periphery of the low pressure anomaly, in which cloud convection was active. In the next afternoon, MCS occurred over the migrated convergence anomaly area. Behavior of the low pressure over the plateau, inducing low-level convergence and formation processes of MCS, was diagnosed by numerical experiment. In the afternoon before the day of MCS genesis, a thermal low occurred over the western TP due to strong surface heating under the dry land condition. Southwesterlies prevailing in the southwestern TP converged with northerlies coupling with upslope wind in the northern slope of the plateau, and this convergence induced low vortex.

The positive vorticity with low vortex propagated to eastern TP due to eastward migration of near-surface westerlies. This migration corresponded to upper enhanced westerlies at the northern part of the Tibetan High, which caused by increase of pressure gradient related to approach of the synoptic trough. In the afternoon of the day of MCS genesis, southwesterlies converged with northerlies in the rear of the propagated low vortex. The convergence allowed formation of an MCS over the eastern TP with wet land-surface condition, where remarkable latent heat flux contributed to moistening of the planetary boundary layer and induced strong convective instability. A sensitivity experiment removing sensible heat flux over the western TP until the day of MCS genesis indicated no-development of thermal low and no-formation of low vortex. Occurrence of the MCS was not simulated due to weakening of low-level convergence without the migrated low vortex condition. On the other hand, MCS was also not formed in another sensitivity experiment removing latent heat flux over the eastern TP on the day of MCS genesis, because drying in the planetary boundary layer caused reduction of convective instability. Then, soil moisture gradation from southeast to northwest was an important function for the MCS formation over the eastern TP.

Based on the numerical simulation study for the WV transport, the pumping up of WV to the same altitude of the plateau surface was attributed to a strong daytime upslope wind. However, the spatial resolution and calculating techniques are insufficient to simulate the detailed structure of the local circulation along with real topography of the Himalayas. In addition, few in-situ observatories are available from which to verify the simulation results. Improved simulation techniques for WV circulation over the steep slopes and their verification

by establishing an observation network are required for further studies.

The passing of the synoptic trough was accompanied by the break phase of the Indian monsoon that causing increase of precipitation to the south of the Himalayas. It is well known that precipitation in the Himalayas mostly occurs in the night, as introduced in Section 1.3. Thus, there must be a strong linkage between enhancement of the nighttime precipitation and prevailing of the WV transport into the TP in the case of the TR type.

The present study revealed the importance of soil moisture gradation from the southeast to the northwest for MCS formation over the eastern TP. The gradation is primarily determined by the occurrence of precipitation in the east produced by the convective activity, including the MCSs themselves. On the other hand, Ueno et al. (2009) pointed out that synoptic scale convergence flowing due to TP topography caused nighttime precipitation in the central TP, which could lead to a northwestward expansion of soil wetness the following morning. As the occurrence of a precipitation system is quite sensitive to sub-plateau-scale surface wetness heterogeneity and also controls the circulation pattern within the plateau, precise information of the surface flux components and their distribution over the plateau is required. Recently, satellite estimation algorithms of the surface flux have been developed [e.g., Ma et al., 2007], and the establishment of stations in the northwestern parts is anticipated to assure the formation of thermal lows.

The stronger westerlies which was migrated the low-level vorticity eastward was one of the highlights to explain the large MCS development. Yamada and Uyeda (2006) and Sugimoto et al. (2008) classified the synoptic condition around the plateau during the monsoon season of

1998 and extracted the pattern of the passing synoptic trough over the central plateau as the “TR type.” In two-thirds of the Large_MCS cases in 1998, a TR case followed within 3 days. This feature suggested that the approach of a mid-latitude synoptic trough would be an important factor in the development of large-scale MCSs in the east. Actually, occurrence number of large sized MCSs increased in the years with prevailing of traveling synoptic trough over the TP, from July through August during 1998 – 2006. Upper westerly jet in the active year of large sized MCS formation was stronger and its position was shifted to south comparing with that in inactive year. Fujinami and Yasunari (2004) showed that sub-monthly variability of cloud convection over the southern plateau was controlled by location of quasi-stationary wave train with wavenumber seven along Asian subtropical jet. Our result of additional analysis of jet track in the active MCS formation year was similar to that in dominant year of submonthly variability shown in them. Activity of mid-latitude wave train covering over the northern TP might determine availability of the low vortex migration, which was necessary to induce low-level convergence and MCS formation over the eastern plateau.

Acknowledgments

I am grateful to the Meteorological Research Institute and Japan Meteorological Agency for permission to use the NHM numerical model. The METEOSAT-5 image was provided by EUMETSAT. The Aqua/AMSR-E Level 2 standard products were provided by Japan Aerospace Exploration Agency (JAXA). GAME reanalysis was provided by Meteorological Research Institute, Japan Meteorological Agency and Earth Observation Research Center/JAXA. JRA25 reanalysis data was provided from the cooperative research project of the JRA-25 long-term reanalysis by the Japan Meteorological Agency (JMA) and the Central Research Institute of Electric Power Industry (CRIEPI). I would like to thank the National Institute for Environmental Studies and the Computer Centers at Tohoku University for using supercomputer.

I would like to show great appreciation to Associate Prof. Kenichi Ueno in University of Tsukuba and Associate Prof. Weiming Sha in Tohoku University who have supported over my research activities in graduated school. I also would like to show special thanks to Dr. Masahiro Sawada in Tohoku University who has taught me technical skill of numerical simulation. I am grateful to Prof. Fujio Kimura, Prof. Yousay Hayashi, Prof. Hiroshi L. Tanaka, Associate Prof. Hiroaki Ueda, Dr. Hiroyuki Kusaka, Mr. Tomoshige Inoue, and Dr. Sachiho Adachi in University of Tsukuba, Prof. Toshiki Iwasaki in Tohoku University, Associate Prof. Nozomu Hirose in Matsue Collage of Technology, Associate Prof. Dai Matsushima in Chiba Institute of Technology, Dr. Akira Noda in Japan Agency for Matine-Earth Science and Technology, and Mr. Masamichi Ohba in CRIEPI for many helpful comments. I acknowledge all student, staff, and involved parties of Atmospheric Science Laboratory in Tohoku University, Climatology and Meteorology group in University of Tsukuba, and Science Grope of Tibetan Plateau meteorology.

References

Barros, A. P., M. Joshi, J. Putkonen, and D. W. Burbank, 2000: A study of the 1999 monsoon rainfall in a mountainous region in central Nepal using TRMM products and rain gauge observations. *Geophys. Res. Lett.*, **27**, 3683-3686.

Barros, A. P. and T. J. Lang, 2003: Monitoring the monsoon in the Himalayas: observations in central Nepal, June 2001. *Mon. Wea. Rev.*, **131**, 1408-1427.

Bollasina, M., L. bertolani, and G. Taritari, 2002: Meteorological observations at high altitude in the Khumbu valley, Nepal Himalayas, 1994-1999. *Bulletin of Glacier Research*, **19**, 1-11.

Chang, C. C., 1981: A contrasting study of the rainfall anomalies between central Tibet and central India during the summer monsoon season of 1979. *Bulletin American Meteorological Society*, **62**, 20-22.

Chen, F., K. Mitchell, J. Schaake, Y. Xue, H. Pan, V. Koren, Y. Duan, M. Ek, and A. Betts, 1996: Modeling of land-surface evaporation by four schemes and comparison with FIFE observations. *J. Geophys. Res.*, **101**, 7251-7268.

Chen, F., and J. Dudhia, 2001: Coupling an advanced land surface-hydrology model with the penn state-NCAR MM5 modeling system. Part 1: Model implementation and sensitivity. *Mon. Wea. Rev*, **129**, 569-585.

Chen, S.-J., and L. Dell'Osso, 1984: Numerical prediction of the heavy rainfall vortex over the Eastern Asia monsoon region. *J. Met. Soc. Japan., 62*, 730-747.

Cheng, Y. W., and W. R. Cotton, 2004: Sensitivity of a cloud-resolving simulation of the genesis of a mesoscale convective system to horizontal heterogeneities in soil moisture initialization.

J. Hydromet, **5**, 934-958.

Ek, M. B., K. E. Mitchell, Y. Lin, E. Rogers, P. Grummann, V. Koren, G. Gayno, and J. D. Tarpley, 2003: Implementation of Noah land surface model advances in the National Centers for Environmental Prediction operational Mesoscale Eta Model. *J. Geophys. Res.*, **108**, 8851, doi:10.1029/2002JD003296.

Evans, L. J., and R. E. Shemo, 1996: A procedure for automated satellite-based identification and climatology development of various classes of organized convection. *J. Appl. Meteor.*, **35**, 638-652.

Fankhauser, C. J., 1974: The derivation of consistent fields of wind and geopotential height from mesoscale rawinsonde data. *J. Appl. Meteor.*, **13**, 637-646.

Fujinami, H., and T. Yasunari, 2001: The seasonal and intraseasonal variability of diurnal cloud activity over the Tibetan Plateau. *J. Met. Soc. Japan.*, **79**, 1207-1227.

Fujinami, H., and T. Yasunari, 2004: Submonthly variability of convection and circulation over and around the Tibetan Plateau during the boreal summer. *J. Met. Soc. Japan.*, **82**, 1545-1564.

Fujinami, H., S. Nomura, and T. Yasunari, 2005: Characteristics of diurnal variations in convection and precipitation over the southern TP during summer, *SOLA*, **1**, 49-52.

Gantner, L., and N. Kalthoff, 2009: Sensitivity of a modeled life cycle of a mesoscale convective system to soil conditions over West Africa. *Q. J. R. Meteorol. Soc.*, **135**, doi:10.1002/qi.425.

Gao, Y., M. Tang, S. Luo, Z. Shen, and C. Li, 1981: Some aspects of recent research on the Qinghai-Xizang Plateau meteorology. *Bull. Amer. Meteor. Soc.*, **62**, 31-35.

Goswami, B. N. and R. S. Ajaya Mohan, 2001: Intraseasonal oscillations and interannual variability of the Indian summer monsoon. *J. Climate,* **14,** 1180-1198.

Hahn, G. D, and S. Manabe, 1975: The role of mountains in the south Asian monsoon circulation. *J. Atmos. Sci.,* **32**, 1515-1541.

Hirose, M., and K. Nakamura, 2005: Spatial and diurnal variation of precipitation systems over Asia observed by the TRMM Precipitation Radar. *J. Geophys. Res.,* **110**, D05106, doi:10.1029/2004JD004815.

Hong, S. and J. J. Lim, 2006: The WRF single-moment 6-class microphysics scheme (WSM6). *Journal of the Korean Meteorological Society*, **42**, 129-151.

Ikawa, M., 1988: Comparison of some schemes for nonhydrostatic models eith orography. *J. Met. Soc. Japan.*, **66**, 753-776.

Ikawa, M., and K. Saito, 1991: Description of a non-hydrostatic model developed at the Forecast Research Department of MRI. *Tech Rep. MRI*, **28**, 238pp.

Inoue, J., 1976: Climate of Khumbu Himal, *Seppyo,* **38**, **special issue**, 66-73.

Kain, J. S., and J. M. Fritsch, 1990: A one-dimensional entraining/detraining plume model and its application in convective parameterization. *J. Atmos. Sci.,* **47**, 2784-2802.

Keshavamurty, R. N., and S. T. Awade, 1970: On the maintenance of the mean monsoon trough over north India. *Mon. Wea. Rev.,* **98**, 315-320.

Koch, E. S., 1984: The role of an apparent mesoscale frontogenetic circulation in squall line initiation, *Mon. Wea. Rev,* **112**, 2090-2111.

Koike, T., Y. Nakamura, I. Kaihotsu, G. Davaa, N. Matsuura, K. Tamagawa, and H. Fujii, 2004:

Development of an advanced microwave scanning radiometer (AMSR-E) algorithm for soil moisture and vegetation water content, *Annual Journal of Hydraulic Engineering*, **48**, 217-222.

Krishnamurti, T. N. and H. N. Bhalme, 1976: Oscillations of a monsoon system. Part I, observational aspects. *J. Atmos. Sci.*, **33**, 1937-1954.

Kurishnamurthy, V., and J. Shukla, 2000: Intraseasonal and interannual variability of rainfall over India. *J. Climate*, **13**, 4366-4377.

Kurita, N. and H. Yamada, 2008: The role of local moisture recycling evaluated using stable isotope data from over the middle of the Tibetan Plateau during the monsoon season. *J. Hydromet*, **9**, 760-775.

Kurosaki, Y., and F. Kimura, 2002: Relationship between topography and daytime cloud activity around Tibetan Plateau. *J. Met. Soc. Japan*, **80**, 1339-1355.

Kuwagata, T., A. Numagiti, and N. Endo, 2001: Diurnal variation of water vapor the central Tibetan Plateau during summer. *J. Met. Soc. Japan.*, **79**, 401-418.

Lau, K. M., and P. H. Chan, 1986: Aspects of the 40-50 day oscillation during the northern summer as inferred from outgoing longwave radiation. *Mon. Wea. Rev.*, **114**, 1354-1367.

Li, C. and M. Yanai, 1996: The onset and interannual variability of the Asian summer monsoon in relation to land-sea thermal contrast. *J. Climate*, **9**, 358-375.

Li, Y. W. Yun, S. Yang, H. Liang, G. Shouting, R. Fu, 2008: Characteristics of summer convective systems initiated over the Tibetan Plateau. Part 1: Origin, track, development, and precipitation, *J. Appl. Meteor. Climatol.*, **47**, 2679- 2695.

Luo, H., and M. Yanai, 1984: The large-scale circulation and heat sources over the Tibetan Plateau and surrounding area during the early summer of 1979. Part Ⅱ: Heat and moisture budgets. *Mon. Wea. Rev,* **112**, 966-989.

Manabe, S., and J. Broccoli, 1990: Mountains and Arid climates of middle latitude. *Science,* **247**, 192-195.

Mapes, E. B., T. T. Warner, and M. Xu, 2003: Diurnal patterns of rainfall in northwestern South America. Part 3: Diurnal gravity waves and nocturnal convection offshore. *Mon. Wea. Rev,* **131**, 830-844.

Moore, T. J., F. H. Glass, C. E. Graves, S. M. Rochette, and M. J. Singer, 2003: The environment of warm-season elevated thunderstorms associated with heavy rainfall over the central United States. *Wea. Forecasting,* **18**, 861-878.

Mujumdar, V. R., U. V. Bhide, S. G. Nagar, S. P. Ghanekar, and P. Seetaramayya, 2005: Thermodynamic characteristics over north Bay of Bengal during active and weak monsoon phases of BOBMEX-1999. *J. Ind. Geophys. Union.*, **9**, 219-233.

Murakami, M., 1976: Analysis of summer monsoon fluctuations over India. *J. Met. Soc. Japan*, **54**, 15-31.

Murakami, M., 1977: Spectrum analysis relevant to Indian monsoon. *Pure and App. Geophys.*, **115**, special issue, 1145-1166.

Murakami, T., 1986: Active and break monsoon, Monsoon. *Tokyodo-syuppan*, Tokyo, JAPAN. pp. 108. (in Japanese)

Murakami, T., 1987: Orography and monsoons, Monsoons. *John Wiley and Sons.*, New York,

United States of America. 331-367.

Murakami, T., and Y. H. Ding 1982: Wind and temperature changes over Eurasia during the easrly summer of 1979. *J. Met. Soc. Japan*, **60**, 183-196.

Numaguti, A., 1999: Origin and recycling process of precipitating water over the Eurasian continent: Experiments using an atmospheric general circulation model. *J. Geophys. Res.*, **104**, 1957-1972.

Ogura, Y., and Y. L. Chen, 1977: A life history of an intense mesoscale convective storm in Oklahoma. *J. Atmos. Sci.*, **34**, 1458-1476.

Ohata, T. K. Higuchi, and K. Ikegami, 1981: Mountain-valley wind system in the Khumbu Himal, east Nepal. *J. Met. Soc. Japan*, **59**, 753-762.

Ohsawa, T., H. Ueda, T. Hayashi, A. Watanabe, and J. Matsumoto, 2001: Diurnal variations of convective activity and rainfall in Tropical Asia. *J. Met. Soc. Japan*, **79**, 333-352.

Onogi, K., J. Tsutsui, H. Koide, M. Sakamoto, S. Kobayashi, H. Hatsushika, T. Matsumoto, N. Yamazaki, H. Kamahori, K. Takahashi, S. Kadokura, K. Wada, K. Kato, R. Oyama, T. Ose, N. Mannoji and R. Taira, 2007: The JRA-25 Reanalysis. *J. Met. Soc. Japan*, **85**, 369-432.

Pant, S. P., 1983: A physical basis for changes in the phases of the summer monsoon over India. *Mon. Wea. Rev.*, **111**, 487-495.

Peilke, A. R., T. J. Lee, J. H. Copeland, J. L. Eastman, C. L. Ziegler, and C. A. Finley, 1997: Use of USGS-provided data to improve weather and climate simulations. *Ecol. Appl.*, **7**, 3-21.

Rao, Y. P. and Ramamurthy, K.S. 1968. *Forecasting Manual Part 1: Climatology of India and Neighborhood—2, Climate of India*, India Meteorological Department, Poona, India.

Ross, B. B., 1987: The role of low-level convergence and latent heating in a simulation of observed squall line formation. *Mon. Wea. Rev*, **115**, 2298-2321.

Sasaki, T., P. Wu, F. Kimura, T. Yoshikane, and J. Liu, 2003: Drastic evening increase in precipitable water vapor over the southeastern Tibetan Plateau. *J. Met. Soc. Japan.*, **81**, 1273-1281.

Sato, T., and F. Kimura, 2005: impact of diabatic heating over the Tibetan Plateauon subsidence over northeast Asian arid region. *Geophys. Res. Lett.*, **32**, L05809, doi:10.1029/2004GL022089.

Sato, T., and F. Kimura, 2007: How does the Tibetan Plateau affect the transition of Indian monsoon rainfall? *Mon. Wea. Rev.*, **135**, 2006-2015.

Segal, M., W. E. Schreiber, G. Kallos, J. R. Garratt, A. Rodi, J. Weaver, and R. A. Pielke (1989), The impact of crop areas in Northeast Colorado on Midsummer mesoscale thermal circulations, *Mon. Wea. Rev*, *117*, 809-825.

Skamarock, W. C., J. B. Klemp, J. Dudhia, D. O. Gill, D. M. Barker, X. Y. Huang, W. Wang, and J. G. Powers, 2008: *A description of the advanced research WRF version 3*. NCAR/TN-475+STR, 113 pp.

Sugimoto, S., K. Ueno, and W. Sha, 2008: Transportation of water vapor into the Tibetan Plateau in the case of a passing synoptic-scale trough. *J. Met. Soc. Japan*, **86**, 935-949.

Sugimoto, S., and K. Ueno, 2009: Formation of mesoscale convective systems over the eastern Tibetan Plateau affected by plateau-scale heating contrasts. *J. Geophys. Res.*, submitted.

Takagi, T., F. Kimura, and S. Kono, 2000: Diurnal variation of GPS precipitable water at Lhasa

in premonsoon and monsoon periods. *J. Met. Soc. Japan.*, **78**, 175-180.

Tao, S., and Y. Ding, 1981: Observational evidence of the influence of the Qinghai-Xizang (Tibet) Plateau on the occurrence of heavy rain and severe convective storms in China. *Bull. Am. Meteorol. Soc.*, **62**, 23-30.

Taylor, M. C., F. Said, and T. Lebel, 1997: Interactions between the land surface and mesoscale rainfall variability during HAPEX-Sahel, *Mon. Wea. Rev*, **125**, 2211-2227.

Taylor, M. C., and T. Lebel, 1998: Observation evidence of persistent convective-scale rainfall patterns. *Mon. Wea. Rev*, **126**, 1597-1607.

Taylor, M. C., D. J. Parker., and P. P. Harris, 2007: An observational case study of mesoscale atmospheric circulations induced by soil moisture. *Grophys. Res. Lett.*, **34**, L15801, doi:10.1029/2007GL030572.

Tian, L., T. Yao, A. Numaguti, and W. Sun, 2001: Stable isotope variations in monsoon precipitation on the Tibetan Plateau. *J. Met. Soc. Japan.*, **79**, 959-966.

Ueda, H., and T. Yasunari, 1998: Role of warming over the Tibetan Plateau in early onset of the summer monsoon over the Bay of Bengal and the South China Sea. *J. Met. Soc. Japan.*, **76**, 1-12.

Ueda, H., H. Kamahori, and N. Yamazaki, 2003: Seasonal contrasting features of heat and moisture budgets between the eastern and western Tibetan Plateau during the GAME IOP. *J. Climate.*, **16**, 2309-2324.

Ueno, K., 1998: Characteristics of Plateau-scale precipitation in Tibet estimated by satellite data during 1993 monsoon season. *J. Met. Soc. Japan.*, **76**, 533-548.

Ueno, K., H. Fujii, H. Yamada, and L. Liu, 2001a: Weak and frequent monsoon precipitation over the TP. *J. Met. Soc. Japan.*, **79**, 429-434.

Ueno, K., R. B. Kayastha, H. M. R. Chitrakar, O. R. Bajracharya, A. P. Pokhrel, H. Fujinami, T. Kadota, H. Iida, D. P. Manandhar, M. Hattori, T. Yasunari, and M. Nakawo, 2001b: Meteorological observations during 1994-2000 at the automatic weather station (GEN-AWS) in Khumbu region, Nepal Himalayas. *Bulletin of Glacier Research*, **18**, 23-30.

Ueno, K., K. Toyotsu, L. Bertolani, and G. Taritari, 2008: Stepwise onset of monsoon weather observed in the Nepal Himalayas. *Mon. Wea. Rev.*, **136**, 2507-2522.

Uppala, M., S., P. W. Kallberg, A. J. Simmons, U. Andrae, V. DA Costa Bechtold, M. Fiorino, J. K. Gibson, J. Haseler, A. Hernandez, G. A. Kelly, X. Li, K. Onogi, S. Saarinen, N. Sokka, R. P. Allan, E. Andersson, K. Arpe, M. A. Balmaseda, A. C. M. Beljaars, L. Vandeberg, J. Bidlot, N. Bormann, S. Caires, F. Chevallier, B. J. Hoskins, L. Isaksen, P. A. E. M. Janssen, R. Jenne, A. P. Mcnally, J. –F. Malfouf, K. E. Trenberth, A. Untch, D. Vasiljevic, P. Viterbo and J. Woollen, 2005: The ERA-40 re-analysis. *Q. J. R. Meteorol. Soc.*, **131**, 2961-3012.

Uyeda, U., H. Yamada, J. Horikomi, R. Shirooka, S. Shimizu, L. Liping, K. Ueno, H. Fujii, and T. Koike, 2001: Characteristics of convective clouds observed by a Doppler radar at Naqu on Tibetan Plateau during the GAME-Tibet IOP. *J. Met. Soc. Japan.*, **79**, 463-474.

Velde, R., Z. Su, M. Ek, M. Rodell, and Y. Ma, 2009: Influence of thermodynamic soil and vegetation parameterizations on the simulation of soil temperature states and surface fluxes by the Noah LSM over the Tibetan plateau site, *Hydrol. Earth Syst. Sci.* **13**, 759-777.

Wang, B., and I. Orlanski, 1987: Study of a heavy rain vortex formed over the eastern flank of

the Tibetan Plateau, *Mon. Wea. Rev.*, **115**, 1370-1393.

Warner, T. T., B. E. Mapes, and M. Xu, 2003: Diurnal pattern of rainfall in northern South America. Part 2: Model simulations, *Mon. Wea. Rev*, **131**, 813-829.

Wu, G. and Y. Zhang, 1998: Tibetan Plateau forcing and the timing of the monsoon onset over South Asia and the South China Sea. *Mon. Wea. Rev.*, **126**, 913-927.

Xu, J., and S. Haginoya, 2001: An estimation of heat and water balances in the Tibetan Plateau, *J. Met. Soc. Japan.*, **79**, 485-504.

Xu, J., S. Haginoya, K. Masuda, and R. Suzuki, 2005: Heat and Water balance estimates over the Tibetan Plateau in 1997-1998. *J. Met. Soc. Japan.*, **83**, 577-593.

Yanai, M., C. Li, and Z. Song, 1992: Seasonal heating of the Tibetan Plateau and its effects on the evolution of the Asian summer monsoon. *J. Met. Soc. Japan.*, **70**, 319-351.

Yanai, M., and C. Li, 1994: Mechanism of heating and the boundary layer over the Tibetan Plateau. *Mon. Wea. Rev.*, **122**, 305-323.

Yanai, M. and G. Wu, 2006: *Effects of the Tibetan Plateau, The Asian monsoon*, Praxis Pulishing Ltd, Chichester, UK.

Yamada, H., and H. Uyeda, 2006: Transition of the rainfall characteristics related to the moistening of the land surface over the central Tibetan Plateau during the summer of 1998, *Mon. Wea. Rev.*, **134**, 3230-3247.

Yamada, H., 2008: Numerical simulations of the role of land surface conditions in the evolution and structure of summertime thunderstorms over a flat highland, *Mon. Wea. Rev.*, **136**, 173-188.

Yamazaki, N., K. Takahashi, and A. Yatagai, 2003: Report on the GAME Reanalysis. *GAME Phase 1 Summary Repport. (GAME Publ. No. 37)*, 81-87.

Yasunari, T., 1979: Cloudiness fluctuations associated with the northern hemisphere summer monsoon. *J. Met. Soc. Japan.*, **57**, 227-242.

Yasunari, T., 1980: A quasi-stationary appearance of 30 to 40 day period in the cloudiness fluctuations during the summer monsoon over India. *J. Met. Soc. Japan.*, **58**, 225-229.

Yasunari, T., 1981: Structure of an Indian summer monsoon system with around 40-day period. *J. Met. Soc. Japan.*, **59**, 336-354.

Yasunari, T., 1998: Toward the implementation of the GAME-IOP 1998 -How is Asian monsoon forced by seasonal change of insolation?-. *Tenki*, **45**, 501-514. (in Japanese)

Yasunari, T., and T. Miwa, 2006: Convective cloud systems over the Tibetan Plateau and their impact on meso-scale disturbances in the Meiyu/Baiu Frontal zone -A case study in 1998-. *J. Met. Soc. Japan.*, **84**, 783-803.

Ye, Duzheng, 1981: Some Characteristics of the summer circulation over the Qinghai-Xizang (Tibet) Plateau and its neighborhood. *Bull. Am. Meteorol. Soc.*, **62**, 14-19.

Ye, D. and G. Wu, 1998: The role of the heat source of the Tibetan Plateau in the general circulation. *Meteorol. Atmos. Phys.*, **67**, 181-198.

Zhang, J., B. Zhu, F. Zhu, D. Weng, G. Sun, J. Lu, Y. Peng, and Y. Wang, 1988: *Advances in the Qinghai-Xizang plateau meteorology*, The Qinghai-Xizang meteorological experiment (1979) and research. Science press, Beijing, 268pp (in Chinese).

Zhu, G., and S. Chen, 2003a: Analysis and comparison of mesoscale convective systems over the

Qinghai-Xizang (Tibetan) Plateau. *Advances in atmospheric science*, **20**, 311-322.

Zhu, G., and S. Chen, 2003b: A numerical case study on a mesoscale convective system over the Qinghai-Xizang (Tibetan) Plateau. *Advances in atmospheric science*, **20**, 385-397.